Summer 8-2022

Measurement of Airborne Radionuclides and Their Relation to Weather Patterns at Orono, ME

James W. Deaton
University of Maine, james.deaton@maine.edu

MEASUREMENT OF AIRBORNE RADIONUCLIDES AND THEIR RELATION TO WEATHER PATTERNS AT ORONO, ME

BY

James William Deaton

B.S. University of Louisiana at Lafayette, 2008

M.S. University of Louisiana at Lafayette, 2010

A DISSERTATION

Submitted in partial fulfillment of the

Requirements for the Degree of

Doctor of Philosophy

(in Physics)

The Graduate School

The University of Maine

August 2022

Advisory Committee:

Charles T. Hess, Professor of Physics, Advisor

George Bernhardt, Research Scientist

Samuel Hess, Professor of Physics

Tom Stone, Adjunct Faculty

Sean Birkel, Research Assistant Professor

MEASUREMENT OF AIRBORNE RADIONUCLIDES AND THEIR RELATION TO WEATHER PATTERNS AT ORONO, ME

BY

James William Deaton

Dissertation Advisor: Dr. Charles T. Hess

An Abstract of the Dissertation Presented
in Partial Fulfillment of the Requirements for the
Degree of Doctor of Philosophy
(in Physics)
August 2022

^{7}Be and ^{210}Pb activities were measured in air sampling filters collected at The University of Maine campus from 2014 to 2019. The activities of ^{7}Be were in the range of 1.178-98.8 Bq, with an average value of 32.13 Bq. The activities of ^{210}Pb were in the range of 0.091 to 13.64 Bq, and an average value of 3.029 Bq. The distributions of activity for both radionuclides are lognormal. Both ^{7}Be and ^{210}Pb show seasonal variation with maximum values in the summer and minimum values in the fall, and the ^{7}Be/^{210}Pb ratio shows a clear seasonal variation with maxima in the spring and summer and minima in the winter. The measured activities of the two radionuclides are correlated ($R=0.593$, $P<0.000001$). There are no significant correlations between the mass of material collected on an air filter and either radionuclide activity, nor are there significant correlations between either mean monthly radionuclide activity and the total amount of precipitation.

These results are compared with a sample of results from the literature, selected for similar latitude, showing consistency with some sampling sites in Europe, notably those with some influence from both oceanic and continental air flows. The likely

mechanism for the seasonal variation in both radionuclides is increased atmospheric mixing in the warmer months, although a possible explanation for the variation in $^{7}Be/^{210}Pb$ ratio is influx of oceanic air at the sampling site during the spring. Further research includes correlating the ^{7}Be data with the 11-year solar cycle and adjusting for its effects, and a more detailed analysis and classification of air flows arriving at the sampling site, and correlation between different air masses (oceanic versus continental, for example) and the measured radionuclide activities.

DEDICATION

In memory of Dr. John R. Meriwether (22 May 1937 – 8 December 2021), for first getting me interested in environmental nuclear physics and its applications.

ACKNOWLEDGMENTS

I would like to thank the US Environmental Protection Agency RadNet program, for allowing the use of their high volume air sampler for all sample collection in this project. I would also like to thank my colleagues in Dr. Hess' lab, John Cummings and Bryn Nugent, who collected and counted the air filters in the 2014 data. I would also like to thank John Cummings and Amber Hathaway for collecting air filters on occasions when I was out of town. My research would not be as complete without their assistance.

I would like to thank my advisor, Dr. Charles T. Hess, for his support throughout my career here at The University of Maine. I would also like to thank Dr. George Bernhardt, for his assistance in writing this dissertation. Long hours of conversations with both of them helped me form my thoughts, and suggested avenues I should pursue in my research or things that I had overlooked. I would like to thank my external reader, Dr. James Kaste, for his feedback on this document. I would also like to thank Mr. Frank Dudish and Mr. David Sturm, for their vocal support of my work as a teaching assistant, and their belief in me as I finished my dissertation.

I would like to thank all my friends in the Department of Physics and Astronomy, especially Sarah Rice, Zach Smith, Alex Khammang, Justin Roundy, Michael Small, and Matt Valles. You all made my time at UMaine a valuable and fun experience, and your friendship through the years has been a continual source of support.

Finally, I would like to thank my family. They have been a constant source of love and support through all my years at the university. My parents provided plenty of advice and stability whenever I needed to vent my concerns, and my dad's knowledge of how to organize a class was invaluable any time I ran into issues as an instructor. My brother has always been one of my best friends, and a source of encouragement and inspiration whenever I needed it.

TABLE OF CONTENTS

LIST OF TABLES

LIST OF FIGURES

CHAPTER 1

INTRODUCTION AND BACKGROUND

1.1 Introduction

Two common airborne radionuclides are beryllium-7 (^{7}Be) and lead-210 (^{210}Pb). Each nuclide is produced by different methods, and has an origin in different parts of the atmosphere. ^{7}Be is produced in the upper atmosphere by spallation interactions between cosmic rays and atmospheric gases. A high energy cosmic ray strikes the nucleus of an atom in the upper atmosphere, and splits it into lighter nuclei. ^{210}Pb is a long-lived daughter of ^{222}Rn, and part of the ^{238}U decay series. Radon produced by radioactive decay in rock and other materials eventually diffuses through the rock and either dissolves in water, or enters a crack or other space, and eventually makes its way to the surface, where it enters the atmosphere. The radon and its progeny are then free to diffuse through the air.

The abundance of each radionuclide in the air, and thus collected via air sampling, is affected by the local weather in various ways. Seasonal variation in the tropopause, the boundary layer between the troposphere and stratosphere, allows the mixing of the two layers, and the introduction of additional ^{7}Be from the upper layers of the atmosphere. Local events such as precipitation can produce a wash-out effect by carrying large amounts of radionuclides to the surface in rain or snow. The abundance of ^{210}Pb can also depend upon the origin of the air mass currently over a region, since the radon concentration over the oceans is much lower than over land. Since the airborne concentrations of these radionuclides can vary with time, and they are used as tracers and for radioactive dating, it is important to have records of the concentrations of these nuclides in the past, present, and future, to ensure they are relatively constant over long time scales.

A long-term study of the airborne radionuclides in the Orono, Maine, area was carried out using an EPA RADNET air sampler located on the roof of Bennett Hall on the University of Maine campus. Bennett Hall is a three story building, so air samples were taken roughly 10 m above the ground. The goal of this study is to determine the effects local weather has on the amounts of each nuclide, and the possible correlations between the two. Due to the different origins of ^{7}Be and ^{210}Pb, it is expected that each is correlated to the weather, but not directly to the other.

1.2 Background

1.2.1 Beryllium-7

Due to its short half-life of 53 days, all ^{7}Be present on Earth is produced recently in the upper atmosphere, by the process of cosmic ray spallation. A definition for spallation reactions from J.-C. David is as follows: a reaction between a fast particle, typically a proton of energy from a few hundred MeV to a few GeV, and an atomic nucleus (David 2015). A high energy cosmic ray particle collides with an atomic nucleus, ejecting fragments such as protons, neutrons and alpha particles, and creating lighter nuclides from the target nucleus. Example reactions studied would be N(p,x)^{7}Be, and O(p,x)^{7}Be (Bodeman et al., 1993, Sisterson et al., 1997). Production cross-section data for ^{7}Be is also available in the graph below, from Yoshimori.

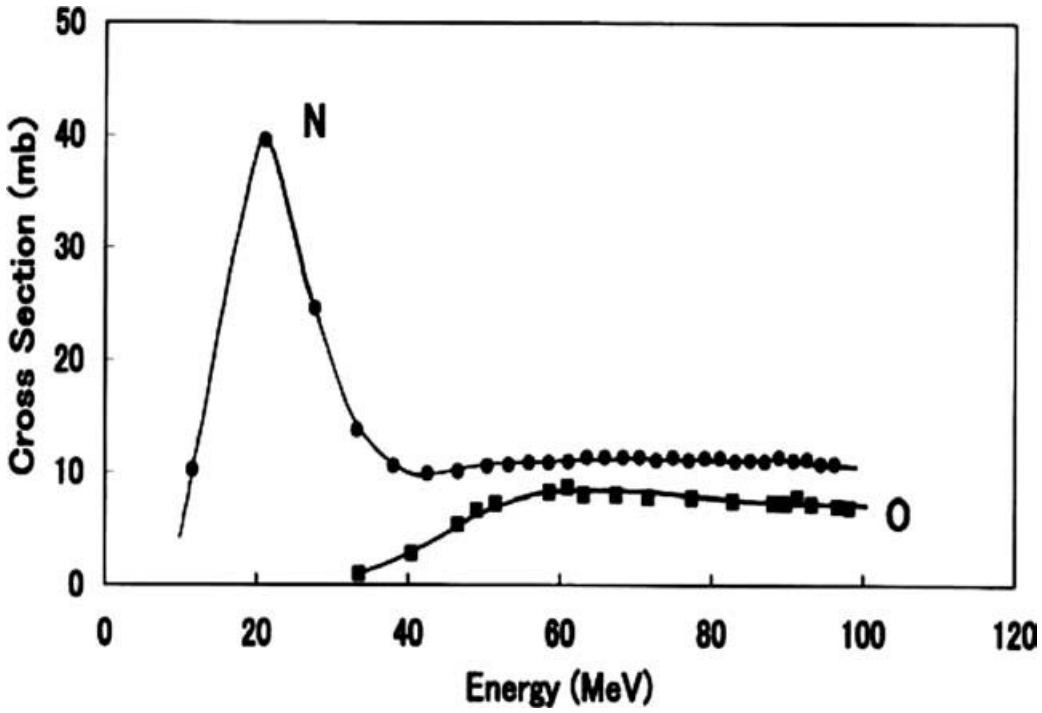

Figure 1.1: p-N and p-O production cross-sections for ^{7}Be plotted against proton energy. (Yoshimori, 2005)

The global average production rate for ^{7}Be is 0.043 ^{7}Be/cm^{2}s. Most ^{7}Be nuclei (around 70%) are produced in the stratosphere, and the rest in the troposphere (Yoshimori 2005). The rate of

production of ^{7}Be depends upon factors influencing the cosmic ray flux to the Earth, such as the 11-year solar cycle, and the Earth's geomagnetic field (O'Brien, 1979, Lal and Peters, 1962). The solar cycle thus also has an affect on the surface air concentration of ^{7}Be (Megumi et al., 2000). The production rate also depends upon the geographic latitude, increasing closer to the geomagnetic poles. Masarik and Beer (1999) provide an illustration of both effects, shown below.

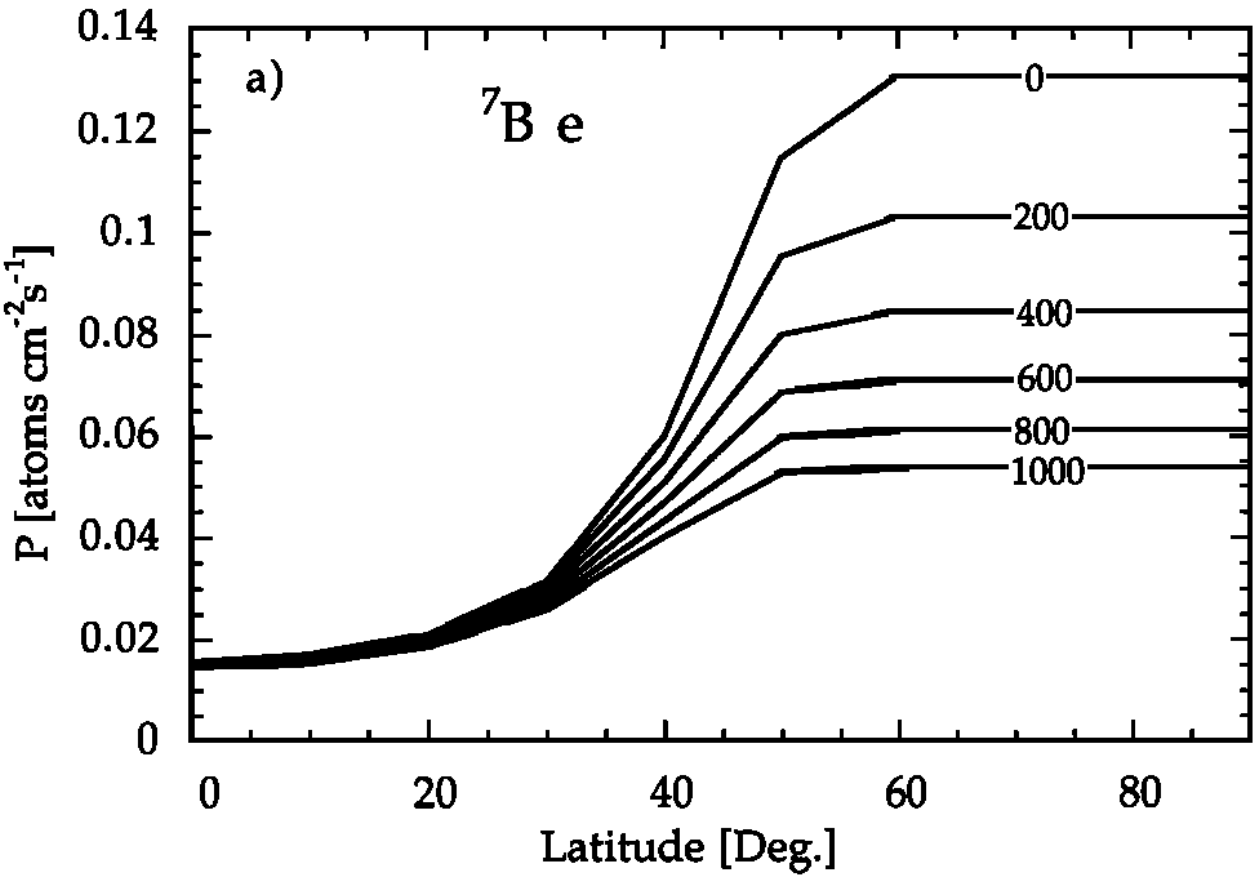

Figure 1.2: Depth-integrated latitudinal production rate for ^{7}Be in the atmosphere for solar modulation parameter Φ = 0, 200, 400, 600, 800, and 1000 MeV (Masarik and Beer, 1999).

The town of Orono is located at roughly 45° North latitude, and can therefore expect variations in the ^{7}Be production rate from 0.09 atoms/cm^{2}s to 0.04 atoms/cm^{2}s depending on the solar cycle, based on the above plot.

After it is produced in the upper atmosphere, the ^{7}Be attaches to a small aerosol particle and transported to the lower atmosphere, eventually brought to the surface by rainfall or other precipitation (Lal and Peters 1962). The global average concentration for ^{7}Be is roughly 4.2 ± 0.4 mBq/m^{3} (Persson, 2015). ^{7}Be is known to vary seasonally, as changes in the local temperature and other weather patterns can affect the permeability of the tropopause, leading to a large transfer of stratospheric air during that time (McHargue and Damon, 1991).

1.2.2. Lead-210

Atmospheric ^{210}Pb is produced by the decay of ^{222}Rn that has entered the atmosphere either through diffusion along cracks and other defects in rock directly to the air, or until it dissolves in water that reaches the surface naturally or via a well, and then exits solution into the air. Since ^{210}Pb has a relatively long half-life of 22 years, it is the primary radon daughter detected in air samples, although shorter-lived daughters can be detected if a sample is counted immediately after collection.

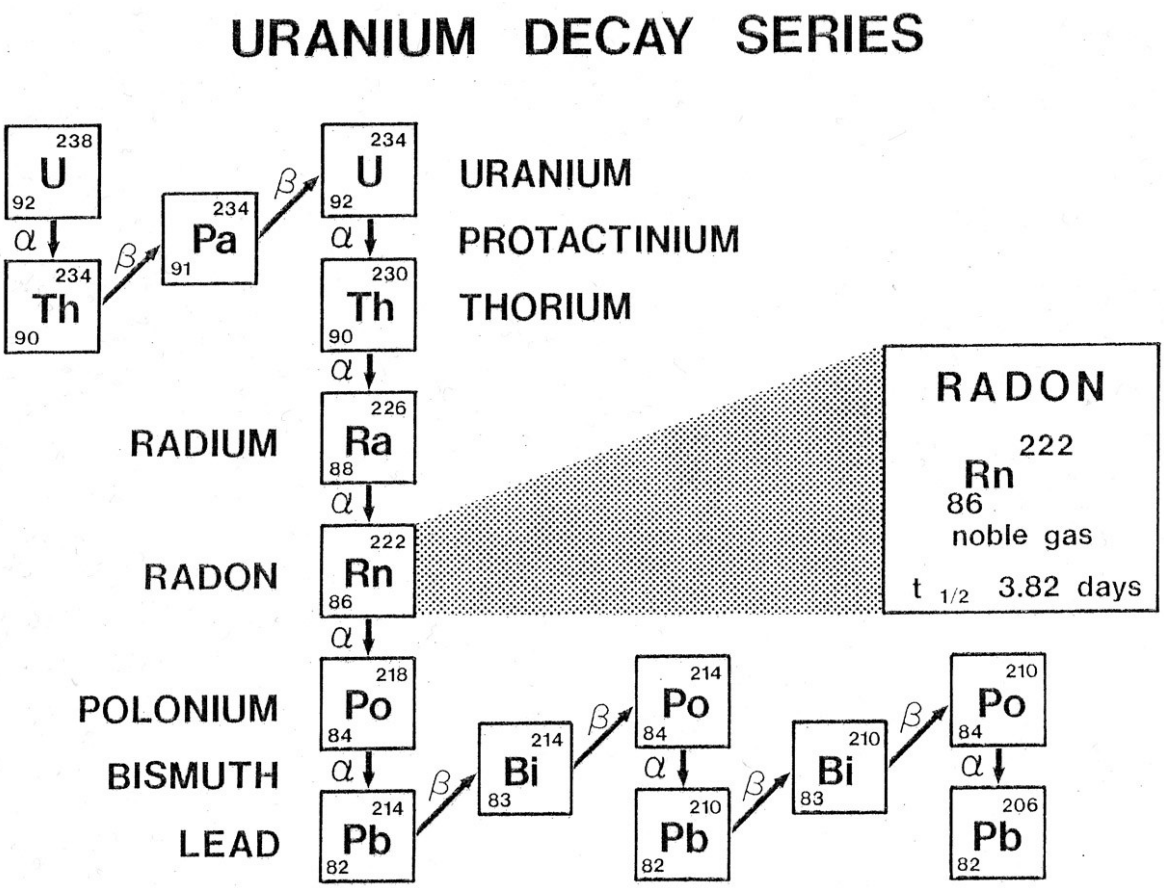

Figure 1.3: ^{238}U (4n+2) decay series, including ^{222}Rn and ^{210}Pb.

^{222}Rn is exhaled from the ground at a rate of roughly 48×10^{18} Bq per year, corresponding to production of atmospheric ^{210}Pb at a rate of 23×10^{15} Bq per year, globally (Persson, 1970, by way of Persson, 2015). The amount of ^{210}Pb deposition in an area depends upon the surrounding surface of the earth and possibilities of exhalation of ^{222}Rn, with the exhalation over sea being small due to the small concentration of ^{226}Ra in seawater (Persson, 2015). Therefore, air masses originating over the oceans are expected to carry lower concentrations of ^{210}Pb than those originating over land.

Both of these nuclides contribute to the yearly background dose a person receives. Radon and its daughters contribute around 68% of the average ubiquitous background dose, around 2.12 mSv per year. Cosmogenic radionuclides, including ^{7}Be, contribute 0.01 mSv per year (National Council on

Radiation Protection and Measurements, 2009). Furthermore, since both nuclides are airborne, they contribute a dose primarily to the lungs, rather than a true full body dose, resulting in an increased risk of lung cancer.

Both nuclides are also used as natural tracers. The presence of ^{7}Be in sediment indicates it is only at most a few months old (around 2 half lives), and it is also used as a tracer for motion of atmospheric air masses and aerosols (Dueñas et al., 2011) or for tracing behavior of novel accumulation-mode aerosol deposition (Landis et al., 2021). For example, data from the Comprehensive Nuclear Test Ban Treaty Organization's International Monitoring System can be used to visualize the locations of the Polar-Ferrel, Hadley-Ferrel, and inter tropical convergence zones (Terzi and Kalinowski, 2017). The ratio of ^{7}Be to ^{210}Pb can also be used as an indicator of whether an air mass is continental or oceanic (Baskaran et al., 1993). Baskaran et al. also show that the strength of the correlation between depositional fluxes of ^{7}Be and ^{210}Pb is different between continental, coastal, and oceanic sampling locations, with stronger correlations in continental locations, and weaker correlations in coastal and oceanic ones.

^{210}Pb is commonly used in radiological dating of sediment, and is accurate for ages up to around 100 years. One of the most common models for ^{210}Pb dating assumes a constant atmospheric flux of ^{210}Pb (Appleby and Oldfield, 1978). Since the amount of ^{210}Pb present in the air varies over time, it is likely not true that the rate of supply from the atmosphere is constant, unless averaged over longer time scales. An alternative model assuming a non-constant rate of supply was recently developed at the University of Maine (Hathaway, 2020), and data on airborne ^{210}Pb may provide insight on possible source functions for the non-constant supply model.

^{210}Pb can also be used as a tracer of areosols, and its long half-life makes it an effective choice for indexing aerosol stable isotopes in long-range transport (Landis et al., 2021). The residence time of ^{210}Pb is often studied using a ratio of parent and daughter isotopes in the decay chain, usually either ^{210}Bi/^{210}Pb or ^{210}Po/^{210}Pb. The resulting residence times often differ between the two ratios, for example 5.6±0.3 days from the ^{210}Bi/^{210}Pb ratio and 19±1 days for ^{210}Po/^{210}Pb (Tokieda et al., 1996). Global simulation of ^{210}Pb gives residence times at northern midlatitudes varying from about 5 days in winter to 10 days in summer (Balkanski et al., 1993). A measurement of the residence time of aerosols carrying ^{7}Be, based upon the mean aerosol growth rate and activity median aerodynamic diameter of aerosol particles gives a residence time of about 7-9 days at temperate latitudes (Papastefanou and Ioannidou, 1995).

1.2.3. Review of atmospheric studies of ^{7}Be and ^{210}Pb.

The town of Orono is located at roughly 44.88° N latitude, 68.67° W longitude, approximately 30 miles (48.3 km) north of the Atlantic coast of Maine. Orono's elevation is 125 feet (38.1 m) above sea level. The results of this study can be compared to those for other parts of New England, and to those in areas with similar climates or at the same latitude. Several examples are summarized below.

Dueñas et al. describe both radionuclides at Málaga, Spain (36° 43' 40" N; 4° 28' 8" W), and their relations to air mass origins. While the location of the Iberian Peninsula is further south, its location near the Atlantic and Mediterranean allow it to show influences from air originating both over continental landmasses and over the ocean. The authors identified and classified several air flows: multiple northwesterly flows of different speeds, south-westerlies, continental north-northeasterly, eastern flows originating over the Mediterranean, and Westerly zonal flows. The northwest and west flows primarily bring in air from the north Atlantic, while the southwest and northern flows bring continental aerosols. Their results show average specific activities of 4.6 mBq m^{-3} for ^{7}Be and 0.54 mBq m^{-3} for ^{210}Pb, with ranges of 2.5-14.9 and 0.24-1.40 mBq m^{-3}, respectively. They show a seasonal

variation of both radionuclides, with an increase in spring and summer, accompanied by increased aerosol mass concentrations, and a moderate association between monthly rainfall and the activities of both radionuclides.

A similar study conducted in central France (45° N) also shows some effects of air mass origin on radionuclide concentration (Bourcier et al., 2011). The air mass origins considered were as follows: marine air masses from the Atlantic, marine-modified masses from the Atlantic that crossed a populated part of northwestern Europe before arriving at the collection site, continental origins to the east of the site, and Mediterranean for air originating from the south of the site. Two sampling stations were employed, one at high altitude, and one at low altitude. The low altitude results are of primary interest for comparison. The monthly averages for each isotope had ranges of 0.33 to 1.13 mBq m^{-3} for ^{210}Pb and 1.73 to 7.73 mBq m^{-3} for ^{7}Be. Both nuclides showed seasonal variation, with ^{210}Pb showing maxima in spring and autumn and a minimum in the winter, and ^{7}Be showing a maximum in summer and minimum in winter. There were no variations of ^{7}Be concentration with air mass origin, but ^{210}Pb showed higher concentrations in continental air masses than in maritime air masses.

In a 2005 study of airborne radionuclides in the Belgrade area (44° 47’ N), Todorovic et al. show the following results. Average monthly concentrations for ^{7}Be ranged from 0.6 to 18.3 mBq m^{-3}, and ^{210}Pb concentrations ranged from 1.09 x 10^{-4} to 30.9 x 10^{-4} Bq m^{-3}. Both radionuclides show seasonal variations, with maximums in summer or early fall and a minimum in winter for ^{7}Be and ^{210}Pb maximums generally observed in the fall. The authors also examine correlations between each radionuclide and the $^{7}Be/^{210}Pb$ ratio with different air stability classes, concluding that the strength of the wind is the main contributor to a significant effect on the air content of the radionuclides.

A study of the Edinburgh (55.9° N) area (Likuku, 2006) provides the following results. Surface air concentrations of 0.01 to 0.74 mBq m^{-3} for ^{210}Pb and 0.63 to 6.54 mBq m^{-3} for ^{7}Be, with averages of 0.21 and 2.50 mBq m^{-3}, respectively. The author uses three-day back trajectories for air mass origins, classifying air masses as either oceanic or continental based on their points of origin. Their results show a decrease of both radionuclides with increased rainfall, and both concentrations showing troughs coinciding with low pressure. ^{210}Pb concentrations are lower in oceanic air, with air masses spending most of their time over the continent showing enriched concentrations. While the data shows some seasonal variation, with a peak in the spring for both nuclides, the author concludes that a larger data set would be needed to make strong conclusions on seasonal influence.

In a 15 year study of ground level air at Thessaloniki, Greece (40° N), Ioannidou et al. report the following results (Ioannidou et al., 2005). The concentrations for ^{7}Be and ^{210}Pb have mean values of 5.02 mBq m^{-3} and 664 µBq m^{-3}, respectively. The ranges for each nuclide concentration are 0.47-12.70 mBq m^{-3} and 108-1982 µBq m^{-3}, respectively. Their data shows the variation of ^{7}Be with sunspot number, with a strong anticorrelation between yearly averaged ^{7}Be concentration and sunspot number. The monthly ^{7}Be concentrations showed a strong seasonal trend with highest values in summer and lowest values in winter. The authors considered contributions from temperature, precipitation, and relatively humidity to the variability of the ^{7}Be concentration, and conclude that only the temperature and sunspot number have a significant effect. The strong dependence on temperature corresponds with the increased vertical transport of air during the warmer months of the year. The monthly mean ^{210}Pb data showed a different seasonal variation, with maxima in the fall and minima in the spring, although the large standard deviations suggest little overall seasonality. The authors propose frequent inversion conditions in surface layer air as a mechanism for the increased ^{210}Pb in he fall. No correlation was found between ^{210}Pb concentrations and air temperature, relative humidity, or rainfall amount.

For comparison with other points in the northeastern United States, a 2013 study by Renfro et al. of the monthly atmospheric fluxes at Stony Brook, New York will be used. The results are as follows. The depositional flux of ^{7}Be had a range of 67 to 395 Bq m^{-2}, with mean value of 229 Bq m^{-2}. ^{210}Pb fluxes ranged from 6.7 to 16.7 Bq m^{-2}, with a mean value of 12.1 Bq m^{-2}. The results show a pattern of increased ^{7}Be deposition flux in the spring and summer and lower values in fall and winter. The $^{7}Be/^{210}Pb$ ratio also showed the same seasonal variation. The flux of both nuclides is positively correlated with precipitation, with ^{7}Be showing a stronger correlation than ^{210}Pb. Measurements taken during individual rainfall events show that the ^{210}Pb flux was deposited early in the event, while the ^{7}Be flux continued sporadically through the event. Since the Stony Brook study measures atmospheric flux rather than concentration, a quantitative comparison will be difficult, but qualitative comparison should still be possible.

CHAPTER 2

METHODS

2.1 EPA RADNET Air Sampler operation

All air samples were collected using an EPA RadNet* air sampling station located on the roof of Bennett Hall, on the University of Maine campus, Orono, ME. The air sampling station consists of a control computer, an air sampling pump, polyester fiber filter, cellular modem, and gamma ray detector. The filters used are 4 inch diameter polyester media, and are greater than 97% efficient for particles 0.2 μm in size or larger (US EPA, personal email communication). In a normal air sampling run, the air sampler is set to collect air for 200 hours (8 days, 8 hours). After the 200 hours has elapsed, the air sampler shuts down, and the filter is collected and replaced with a fresh filter. The start and end date and time of the run is provided by the onboard software, as is the total sample volume, in m^3. When an air filter is collected, it is placed in a wax paper bag. The start and stop time for each run is recorded, as is the time the filter was collected (if different from the stop time for the run), and the total sample volume. The average sample rate is on average 60 m^3/hour, leading to a total sample volume of roughly 12,000 m^3 for a full 200 hour run.

While the air sampler has a battery back-up power supply (a commercially-available CyberPower model 850PFCLCD, at the time the data was collected), in the event of power failures disrupting a sample in progress, the sampling program was restarted remotely by the EPA once power had returned and the air sampler was again communicating. Usually, this results in either lower overall sample volumes. Sometimes when the sampling program is reset remotely, the start, stop, and sample volume data displayed will not be correct. A full list of start time, stop time, and sample volume data for the time of the experiment has been requested from the EPA.

---

* US EPA, Office of Radiation and Indoor Air, Radiation Protection Division, 1200 Pennsylvania Avenue, NW, Washington, DC 20460

Figure 2.1: EPA RADNET air sampling station on the roof of Bennett Hall.

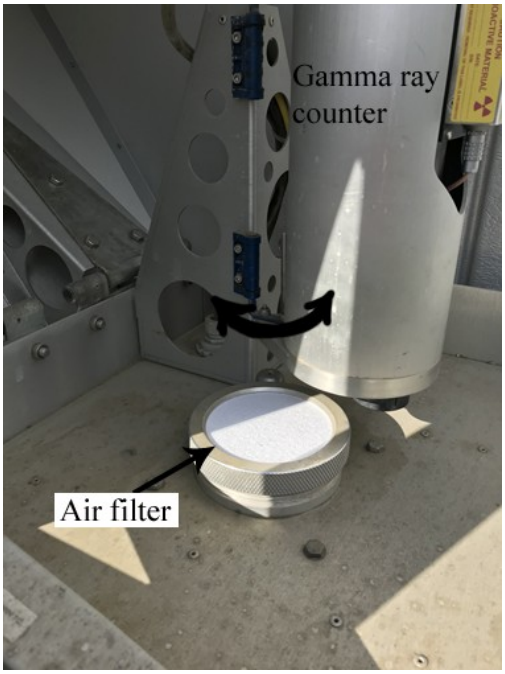

Figure 2.2: Air filter loaded into the air sampler. The gamma detector used as part of the RADNET system for semi-real time monitoring can be moved above the filter during operation. It is shown moved to the side, for ease of replacing a filter.

2.2. Gamma ray counting of air filters

After a run is complete, the air filter is collected and counted with a CANBERRA* XtRA high-purity germanium gamma ray detector (model GX10023). The model detector used has 100% relative efficiency, and uses a thin aluminum window which extends the useful energy range down to 3 keV. The detector is encased in a 2000 pound aged lead shield, graded with copper on the interior to further reduce background from the shield itself.

The gamma detector is connected to a CANBERRA model 2002X preamplifier, that connects to the +4000V bias supply (ORTEC† model 459 0-5kV bias supply) and CANBERRA Model 2010 spectroscopy amplifier. Typical settings for the amplifier are as follows: Coarse gain: 30, Fine gain 7.20, Shaping time 8 μs, Restorer aysmmmetric, HI; 100 mV threshold, input polarity positive, output polarity positive. The spectroscopy amplifier is connected to an AMETEK ORTEC Easy MCA multichannel analyzer connected to a PC via USB. Each filter's gamma ray spectrum is collected and analyzed on a PC running ORTEC MAESTRO software. Each spectrum is saved with a fliename specifying the end date of the filter's air sampling run in YYYYMMDD format.

* Mirion Technologies, 800 Research Parkway, Meriden, CT 06450
† Advanced Measurement Technology, 801 South Illinois Avenue, Oak Ridge, TN 37830

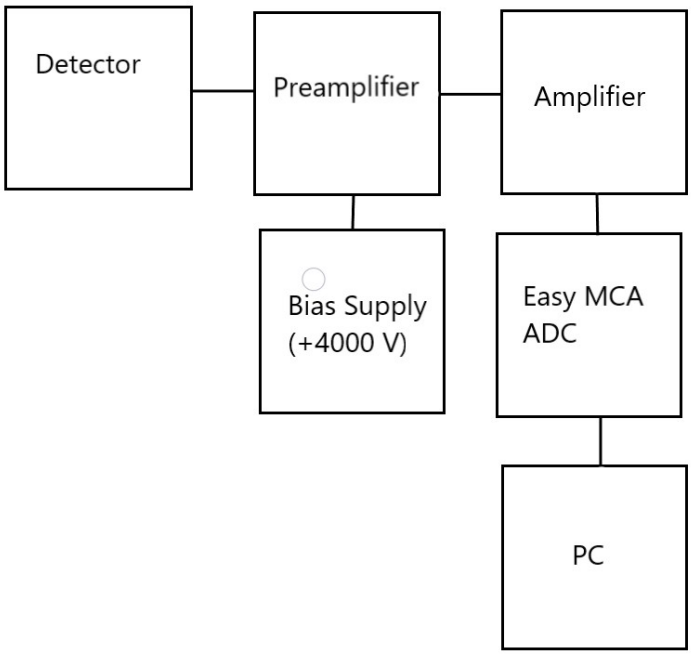

Figure 2.3: Electronics block diagram for the gamma ray counting system.

To count each sample, the filter is placed in a wax paper envelope after collection. The envelope is then placed in a plastic bag attached to the end of a 1 L nalgene bottle, and the bottle is placed in the shielded counting chamber for the detector, positioned so that the filter is against the front surface of the detector. Counts taken prior to November 13, 2015 were taken with the air filter approximately 5 cm away from the detector. The air filters are counted for either 6 or 12 hours, with 12 hours as the preferred count time. All data is normalized to count rate to avoid issues with different counting times for different samples. In cases where multiple air filters were run (see section on air filter efficiency below), each air filter was counted individually for comparison, and also counted together, for a measurement of the total radioactivity collected on both filters. In such cases, the data from both filters counted together were used for the radiological data over time.

Figure 2.4, Left: The horizontal gamma ray detector used in counting all air filters, showing the shield from the outside. Figure 2.5, Right: The interior of the shield, showing the detector and nalgene bottle.

Figure 2.6, Left: Air filter in its wax paper envelope, mounted on the nalgene bottle for counting.

Figure 2.7, Right: Air filter and bottle in counting chamber, pressed against the detector.

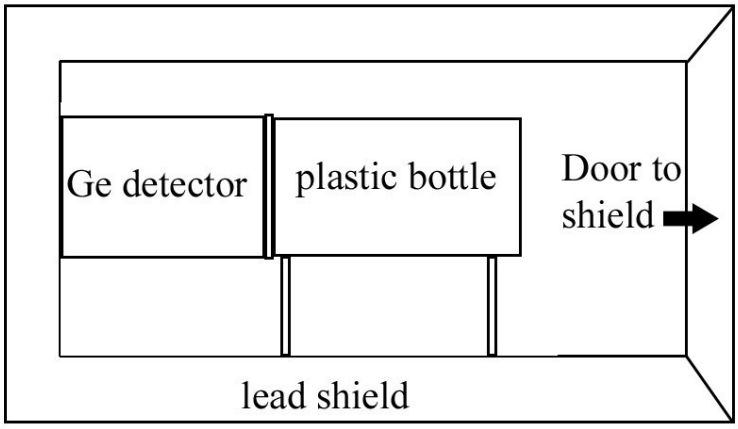

Figure 2.8: Sketch of the counting geometry, showing the filter pressed against the detector inside the shield.

2.3 Analysis of gamma spectrum data

The data is analyzed in ORTEC MAESTRO software version 7.01 (copyright Advanced Measurement Technology, Inc, 2012), a commercially available multi-channel analyzer emulator software package. Data collection is controlled in MAESTRO, with manual start and stop buttons, and pre-set total live time of 12 hours (43,200 s). The number of counts in a specific channel represents the voltage pulses of a certain height from the spectroscopy amplifier, and once the spectrum is calibrated in the program, gammas at a specific energy.

There are two ways to find the net counts in a peak for a specific gamma energy. The first is to select a region of interest (ROI) and selecting the built-in Sum option. The second is to manually locate the desired peak and follow the following steps:

- Locate the peak at the energy of interest, and place the vertical marker at the channel on the center of the peak. Record the channel number for the center of the peak.
- Record the number of counts in the center channel and add them to the counts of each channel to the left and right that makes up the peak. Peak widths are typically 3 to 5 channels.

- Create an average background by recording the counts in the same number of channels to the left and right of the peak as the number of channels in the peak, adding them up, and dividing by two. For example, if the peak is five channels wide, five channels on either side of the peak would be summed for the background.
- Subtract the background from the peak counts.

To avoid issues with drifting calibration, the ROIs marked for the Sum option were marked by hand on the individual spectrum files when the peak counts were recorded, rather than marked once and left for all data runs. The location of the peaks for all hand-calculated peak areas was also tracked, and showed very little drift over time.

Once the net peak counts are determined, the uncertainty in the peak is calculated. In the case of the software's Sum option, an uncertainty is provided. If the peak counts are found by hand, the uncertainty is found by the square root of the number of counts. Each number of counts is divided by the total counting time in seconds to produce a count rate for each isotope in each filter. To go from count rate to activity, the count rates are divided by the branching ratio for gamma rays for each isotope (0.0418 for ^{210}Pb and 0.1032 for ^{7}Be), and by the efficiency of the detector at each gamma ray energy. In cases where the air filter was not counted at the time of collection, the ^{7}Be (half life of 53.22 days) may have decayed significantly since the time the filter was collected. Therefore, the activity of ^{7}Be at the time of collection was determined by back-calculation using the time between collection and counting in days. Due to its much longer half life (22.2 years), no such calculations were made for ^{210}Pb. Several background counts were also taken, for comparison with all filter spectra. Notably, there is a background ^{210}Pb peak, most likely due to lead contained in the shield, and the average count rate is 0.004951 counts per second. This count rate corresponds to a value of roughly 214 counts in a 12 hour counting period. This count rate will be subtracted from all ^{210}Pb count rates before calculating activity.

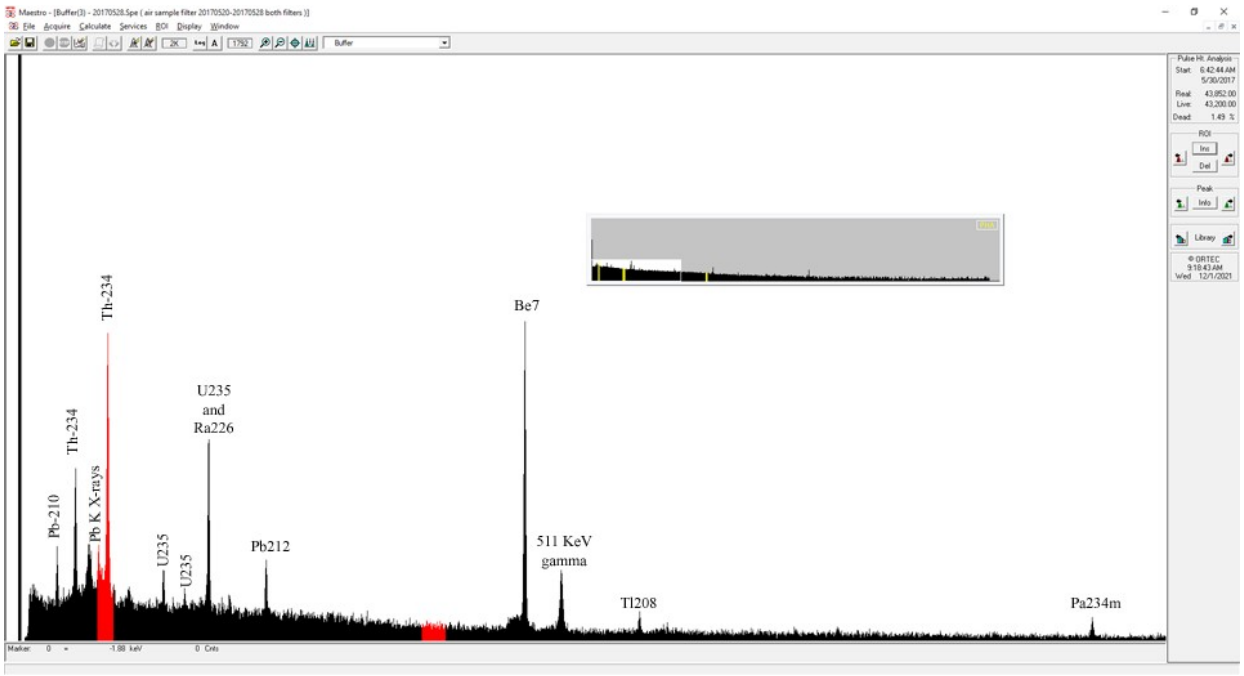

Figure 2.9: Example of MAESTRO recalled spectrum for one of the air filters. Areas marked in red are marked Regions of Interest. The visible peaks are labeled.

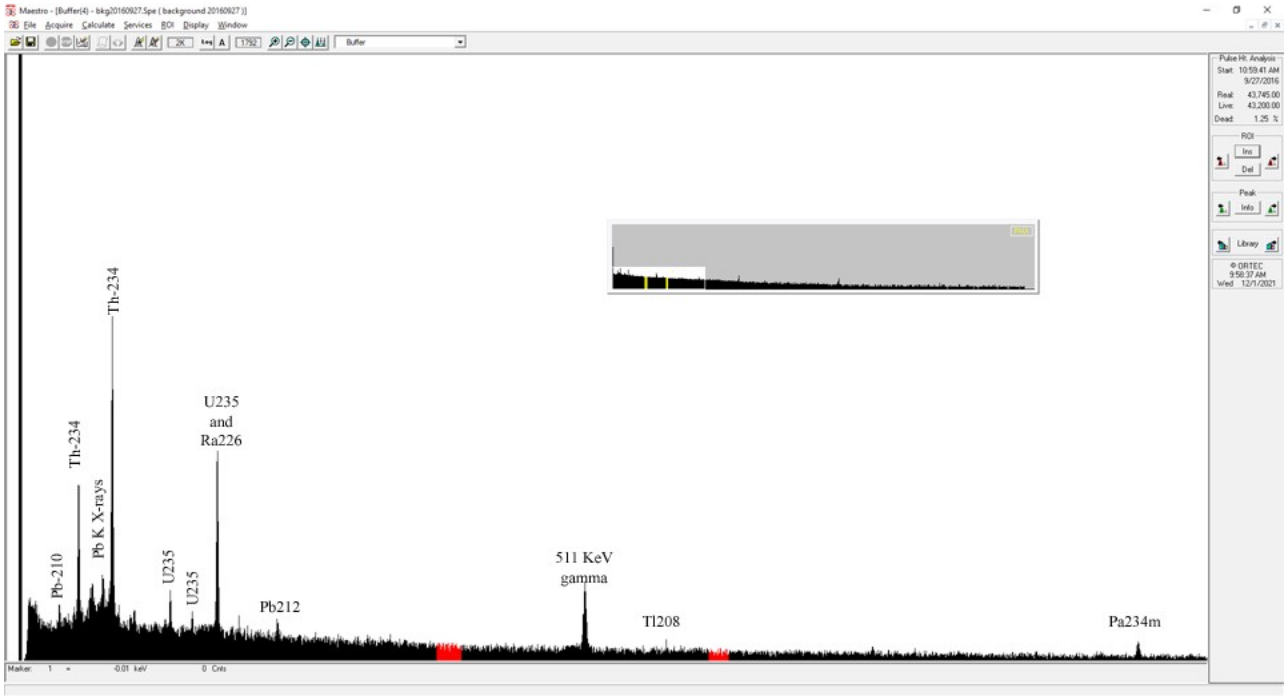

Figure 2.10: Background spectrum on MAESTRO, for comparison with the above spectrum for the air filter. Both spectra show the same region, with the same vertical scale.

2.4 Calibration and Counting Efficiency

The gamma ray spectrum in MAESTRO is calibrated using a standard filter provided by the US EPA. The standard, originally reference dated at 1-May-2007, only contains detectable amounts of ^{210}Pb, ^{137}Cs, and ^{60}Co, as all other isotopes used in the initial preparation of the sample have decayed considerably from their initial activities. The activities on production are 80.79 nCi, 5.421 nCi, and 9.269 nCi, respectively. The standard is an air filter provided by the EPA, prepared with evaporated metallic salts of the isotopes listed below, and sealed in a Kapton (polyimide) sandwich (Eckert & Zeigler Certificate of Calibration, May 2007).

Table 2.1: Nuclides and activities contained in calibration filter, from Certificate of Calibration Multinuclide Standard Source (Eckert & Zeigler Isotope Products, reference date May 1, 2007 12:00 PST).

Gamma-Ray Energy (keV)	Nuclide	Half-Life	Branching Ratio (%)	Activity (nCi)	Gammas per second	Total Uncertainty
47	Pb-210	22.3 years	4.18	80.97	124.9	7.0 %
88	Cd-109	462.6 days	3.63	66.24	88.97	3.1 %
122	Co-57	271.79 days	85.6	4.433	140.4	3.1 %
166	Ce-139	137.640 days	79.9	5.241	154.9	3.0 %
392	Sn-113	115.09 days	64.9	15.27	366.7	3.0 %
662	Cs-137	30.17 years	85.1	5.421	170.7	3.1 %
898	Y-88	106.630 days	94.0	15.77	548.5	3.0 %
1173	Co-60	5.272 years	99.86	9.269	342.5	3.0 %
1333	Co-60	5.272 years	99.98	9.269	342.9	3.0 %
1836	Y-88	106.630 days	99.4	15.77	580.0	3.0 %

To obtain an efficiency curve, the standard source was counted for 600s, and the total counts in each peak for ^{210}Pb, ^{137}Cs, and ^{60}Co were determined by Compton background subtraction. The activity of each isotope in Bq was calculated using the total time elapsed between May 2007 and June 2016, a period of 6.0821 years. The activities at counting were calculated as 2474.32 Bq ^{210}Pb, 174.49 Bq ^{137}Cs, and 154.41 Bq ^{60}Co. Only long-lived nuclides were considered, as it was assumed that most others will have decayed below detectable levels in the intervening time. Total gammas in 600s were calculated for each isotope using the activity and branching ratio for gammas for each isotope, and used to determine a counting efficiency factor for each isotope. These counting efficiencies were then plotted on a semi-log plot against gamma ray energy. One set of data and efficiency plot was created for the filter 5 cm from the detector, and another for the filter pressed against the detector.

2.5. Air Filter Collection Efficiency

In addition to the counting efficiency for the counting geometry used, the efficiency of the air filters themselves was also investigated. If the efficiency is relatively low, then it would be important to account for it in any attempts to calculate the airborne concentrations of each nuclide. To test the efficiency of the filters used in the air sampler, two filters were stacked on top of each other, instead of the single filter usually used in standard operation. A separate test was also made using three filters.

The model for finding the efficiency of the air filters assumes an initial amount of material I, and an efficiency for collecting material of α. The amount deposited in the first filter the air passes through will be equal to $I\alpha$, and the air passing on through the second filter will have a remaining amount of $I(1-\alpha)$. The second filter, assuming the same efficiency, will collect material equal to $I(1-\alpha)\alpha$.

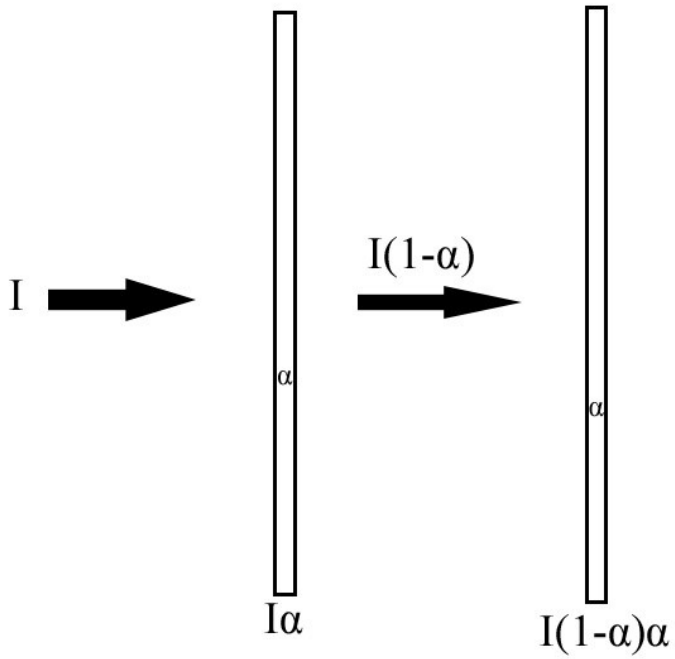

Figure 2.11: An illustration of the material collected by each filter in sequence, as described above.

To solve for α, a ratio of the deposited amounts of each filter can be constructed: $\frac{I\alpha}{I\left(\alpha-\alpha^2\right)}$. This fraction reduces to $\frac{1}{1-\alpha}$ and will be equal to the ratio of the net counts or count rate for a given material in the first filter to that of the second filter. Therefore, $\frac{1}{1-\alpha}=\frac{top\ filter\ counts}{bottom\ filter\ counts}$ and solving for α yields $\alpha=1-\frac{bottom\ filter\ counts}{top\ filter\ counts}$.

Several measurements for α were taken using two filters stacked in this way, with the filter placed on top marked with a small dot of ink at the edge, so it could be easily identified even after the filters were separated. Each filter was counted for 12 hours. Both filters were also counted together for data on the total activity of ^{210}Pb and ^{7}Be collected in the sampling run, and this data was used in the

ongoing plots of activity over time. When determining ^{210}Pb counts, the average background count for ^{210}Pb is subtracted from both values.

An attempt was made to use a stack of three filters. Although no issues were presented for air flow through the filters, the gamma counting for the second and third filters down the stack showed a very small, broad peak for ^{210}Pb that was already near the background. While it is likely that the issue was primarily due to a low overall ^{210}Pb activity present in the air at that time (July, 2016), a second attempt at three filters was not made.

2.6. Mass collected by filters

From late September, 2015 to the end of November 2017, data was collected to study the effect the collected mass of material might have on the radioactivity detected on each filter after an air sampling run. Before the run, the filters were massed using a H&C Weighing Systems model M124A electric precision balance, sensitive to 0.0001 g. After each air sampling run, the date the filter was collected was recorded, and the filter was massed a second time using the same scale. The mass of suspended air particles caught in the filter was determined by subtracting the filter's initial mass from its mass after the air sampling run.

The standard deviation of all initial filter masses was calculated as ±0.231 g, roughly 5.68% of the average mass of a filter. With the resulting data, a plot of material collected over time was constructed, and the activity of radoiosotopes was also plotted against the collected mass. The activities were also normalized to specific activity (in Bq/g) by dividing by the collected mass and examined by plotting the specific activity values over time. First, all data was considered, then data from filters whose final measured mass after the air sampling run were within one standard deviation of the original filter mass were rejected, and a second set of plots was made.

CHAPTER 3

RESULTS

3.1 Calculating Counting Efficiency

The calibration of detector counting efficiency data are presented first, since the resulting efficiency values for the air filter geometry are used to calculate the activity of nuclides present on each air filter. The tables below show the data for counting the standard filter prepared for the EPA by Eckert & Zeigler. Tables 3.1-3.3 show the net counts in each peak, total decays for each nuclide over the counting time, total gamma rays counted, and the calibration constant in counts per gamma ray released by the material.

The total decays were calculated using the activity of each nuclide in Bq as calculated at the time of counting and the total counting time. The activities are 2474.32 Bq ^{210}Pb, 174.49 Bq ^{137}Cs, and 154.41 Bq ^{60}Co. Since the counting times are very small relative to the half-lives of each nuclide, the activity can be treated as constant over the counting interval, and total decays found by multiplying the activity by the counting time.

One count, with the filter pressed against the detector, was taken for the full 43200 second count time used for most of the air sample filters, and gives uncertainties of 0.286 % to 0.136 %. The 3600 second runs have uncertainties on the order of 1% for the peaks with smaller total counts, and are considered an acceptable trade-off between time taken per run and counting statistics. The efficiencies below are calculated as counts per gamma ray emitted by the source.

Table 3.1: Count rate, decays/count (Bq/cps), and counts/gamma (cps/gamma per second) for 43200 second live time run, filter pressed against detector.

Nuclide	Count rate (cps)	Decay/count	Count/gamma
Pb-210	12.55	197.21	0.1214
Cs-137	8.52	20.47	0.0574
Co-60	3.14	49.07	0.02041
Co-60	2.84	54.36	0.01843

Table 3.2: Count rate, decays/count (Bq/cps), and counts/gamma (cps/gamma per second) for 3600 second live time run, filter 1 cm from detector.

Nuclide	Count rate (cps)	Decay/count	Count/gamma
Pb-210	12.76	193.941	0.1289
Cs-137	8.37	20.84	0.0564
Co-60	3.43	44.99	0.02228
Co-60	3.08	50.04	0.01999

Table 3.3: Count rate, decays/count (Bq/cps), and counts/gamma (cps/gamma per second) for 3600 second live time run, filter 5 cm from detector.

Nuclide	Count rate (cps)	Decay/count	Count/gamma
Pb-210	6.71	368.771	0.0678
Cs-137	3.90	44.6878	0.0263
Co-60	1.80	85.5007	0.0117
Co-60	1.58	97.5041	0.0103

While the counting efficiency for ^{210}Pb can be obtained directly from the above data, ^{7}Be must be extrapolated from the existing data, as no prepared standard of known activity was used. By plotting the efficiency data versus gamma ray energy, an efficiency curve can be constructed and the efficiency at points not directly measured can be estimated for this counting geometry.

Data of this kind can be fitted with a variety of models, typically a high order polynomial of a form such as $\ln(\varepsilon) = C_0 + C_1 \ln(E) + C_2 (\ln(E))^2 + C_3 (\ln(E))^3 + C_4 (\ln(E))^4 + C_5 (\mathrm{Ln}(E))^5$ (McFarland, 1991) or $\epsilon(E) = \frac{P_1 + P_2 \ln(E) + P_3 \ln(E)^2 + P_4 \ln(E)^3 + P_5 \ln(E)^4}{E}$ (Alnour et. Al, 2014), where ε is the efficiency, E is the gamma energy, and C_i and P_i are fitting parameters for each model. Such approaches typically require more data points than there are fitting parameters, spanning the entire energy range of interest. Such a case is not available here, as many of the nuclides in the standard filter used had decayed away. An attempt was made to fit the data in Matlab, but did not provide reasonable predictions for the efficiency of the 477 keV ^{7}Be gamma, likely due to a lack of data points in the 100-500 KeV range. Instead, a hand-drawn plot and fit of the data will be used.

The efficiencies for ^{210}Pb have been measured directly and are 0.1214 counts/gamma when against the detector, and 0.0678 counts/gamma when 5 cm away from the detector. The efficiency for the 477.6 KeV gamma from ^{7}Be is roughly 6.5% for the filter pressed against the detector, and 2.66% at 5 cm from the detector. These numbers will be used in finding the activity based on counts below.

3.2 Air Sampling Data

3.2.1 Data analysis and time series

Tables 3.4 and 3.5 below show a representative sample of the data processed from the MAESTRO spectra for each filter. Full data tables showing the activity of each nuclide and their uncertainties are available in Appendix A. The spreadsheet file containing all the data as shown in these tables is also included as part of the digital files.

Table 3.4: First half of the processed spectroscopy data.

Sample End Date	Date Filter Counted	^{210}Pb Gross Counts	^{210}Pb Background	^{210}Pb Net Counts	^{7}Be Gross Counts	^{7}Be Background	^{7}Be Net Counts
2/13/2014	7/24/2014	883	353.5	529.5	459	145	314
2/27/2014	7/15/2014	968	374.5	593.5	738	163.5	574.5
3/16/2014	7/14/2014	716	351.5	364.5	710	153	557
3/28/2014	7/11/2014	989	362	627	1216	211	1005
4/9/2014	7/10/2014	738	371.5	366.5	1155	204	951

Table 3.5: Second half of the processed spectroscopy data. The time in days between the end date of air sampling and the date the air filter is counted is used to find the ^{7}Be activity at the end of the air sample run.

^{210}Pb Uncertainty (%)	^{7}Be Uncertainty (%)	^{210}Pb counts per second	^{7}Be counts per second	^{210}Pb Activity (Bq)	^{7}Be Activity (Bq)	Time between collection and counting (days)	^{7}Be Activity (Bq) back-calculated for time elapsed
6.1	7.3	0.0196	0.0145	3.631	2.167	161	17.59
5.7	5.0	0.0225	0.0266	4.181	3.965	138	23.86
8.2	5.0	0.0119	0.02548	2.213	3.844	120	18.31
5.5	3.6	0.0241	0.0465	4.469	6.936	105	27.17
8.3	3.7	0.0120	0.0440	2.230	6.563	92	21.71

The uncertainties are calculated using the square root of the gross peak counts plus half the background count used in Compton subtraction, giving a value of the counting uncertainty. This value is then converted into a percentage of the net counts in each peak, for ease of propagating to other values derived from the net counts. Counts per second are found by dividing the net peak counts by the total counting time, to normalize for different counting times. Activity is calculated using the efficiencies above in counts per gamma and the branching ratio for gamma ray emission for each isotope as follows: $\frac{Counts\ per\ second}{Efficiency * Branching\ ratio}$, using the branching ratio for gamma ray emission for each nuclide. The branching ratios used are 4.18% for the 47 keV ^{210}Pb gamma, and 10.32% for the 477 keV ^{7}Be gamma. In the case of ^{7}Be, the time between filter collection and counting was, for the earlier samples, on the order of one or more half lives, so the activities measured are back-calculated to the activities at the time of collection, using $A_0=Ae^{\lambda t}$, where A_0 is the initial activity, A is the activity at the time of counting, λ is the radioactive decay constant in $(days)^{-1}$, and t is the time in days between collection and counting. For each activity of each nuclide, an uncertainty was calculated by multiplying activity by the percent counting uncertainties for the corresponding peak.

Figures 3.1 and 3.2 show the activity results, with uncertainties, plotted over time. Figure 3.1 shows all the data on a single plot, while figure 3.2 splits the data roughly by year, for ease of examination. In both figures, the ^{7}Be data is plotted in blue, on the left-hand y-axis, and the ^{210}Pb data is plotted in black, along its own right-hand y-axis. The data are not plotted in the same scale to better show the variations in ^{210}Pb activity, since it is roughly an order of magnitude smaller than the ^{7}Be data, and variations would largely be lost if all data were plotted at the scale needed to show the variations in the ^{7}Be activity.

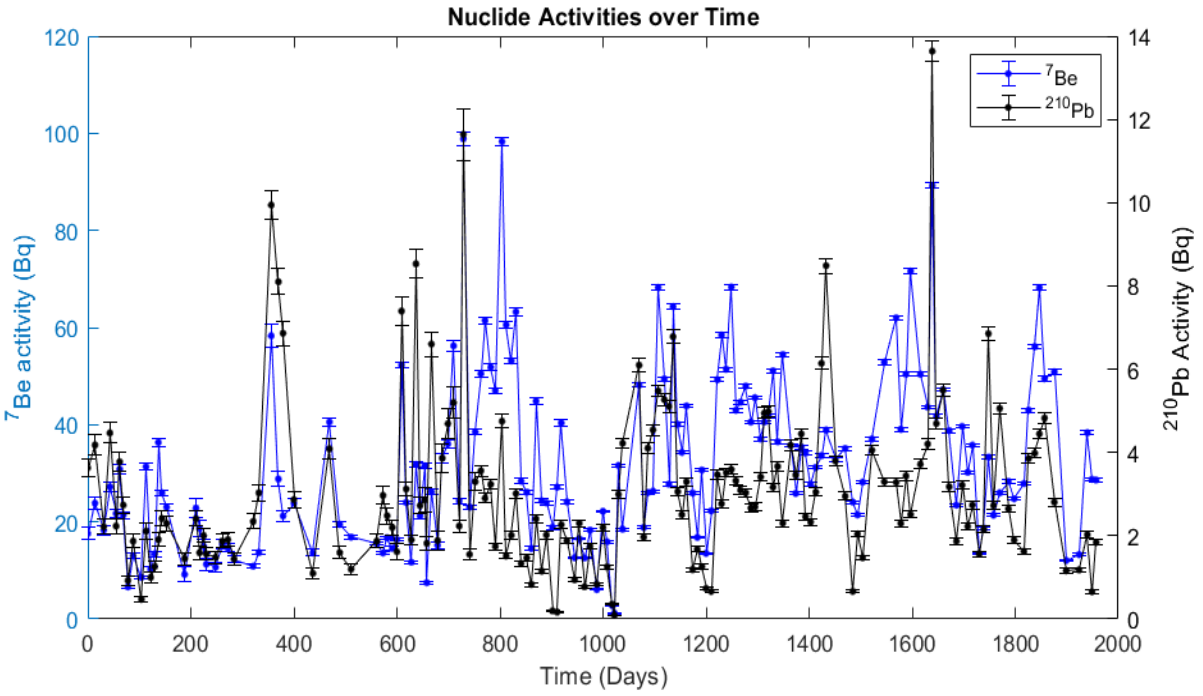

Figure 3.1: ^{7}Be and ^{210}Pb activities over time, showing all data points. See Appendix 2 for larger reproductions of these full graphs. Note that the scale on each y axis is not the same, the ^{210}Pb activities are roughly one order of magnitude smaller than the ^{7}Be data. On the x-axis, t = 0 corresponds to the sample end date of the first filter in the data set, February 13, 2014. The end point of the data set is at June 24, 2019, 1957 days later.

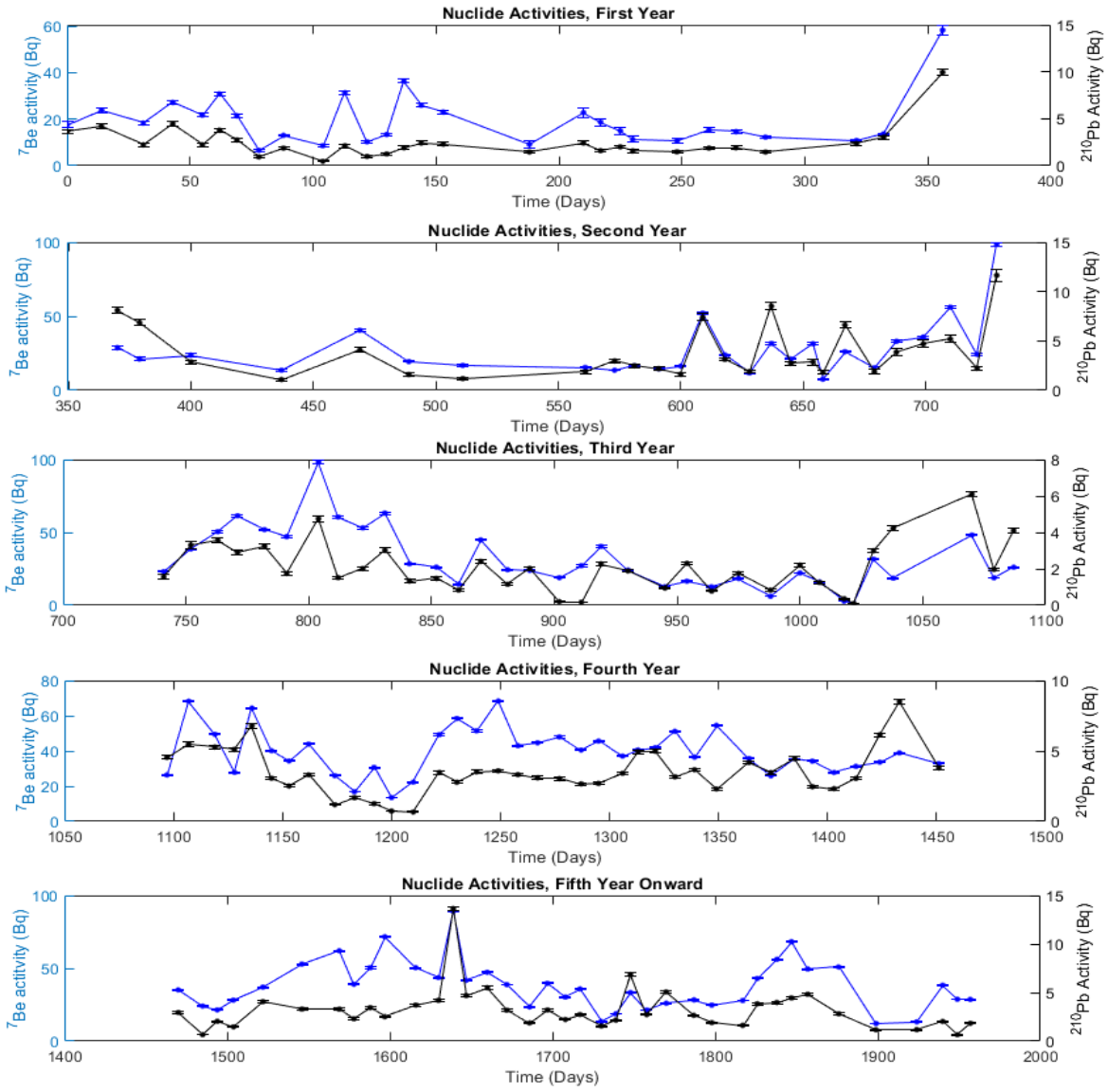

Figure 3.2: ^{7}Be and ^{210}Pb data over time, split into roughly year-long segments. As in the previous plot, ^{7}Be is plotted in blue, and ^{210}Pb plotted in black.

The range of values for each nuclide are 0.0907 to 13.64 Bq for ^{210}Pb and 1.178 to 98.84 Bq for ^{7}Be. The arithmetic means for each data set are 3.029 Bq and 32.13 Bq for ^{210}Pb and ^{7}Be, respectively. The standard deviations from the mean are 2.05 Bq and 17.9 Bq, respectively. Histograms of the data show a clear lognormal distribution for both the ^{7}Be and ^{210}Pb activities, as reported in the literature (Todorovic et al., 2005, Likuku, 2006). The Pearson correlation coefficient, as calculated by Matlab, between the lead and beryllium activities, is 0.5932, with a p-value of $7.2243*10^{-17}$, much smaller than the significance level of 0.05, suggesting that the correlation between the two nuclide activities is significant.

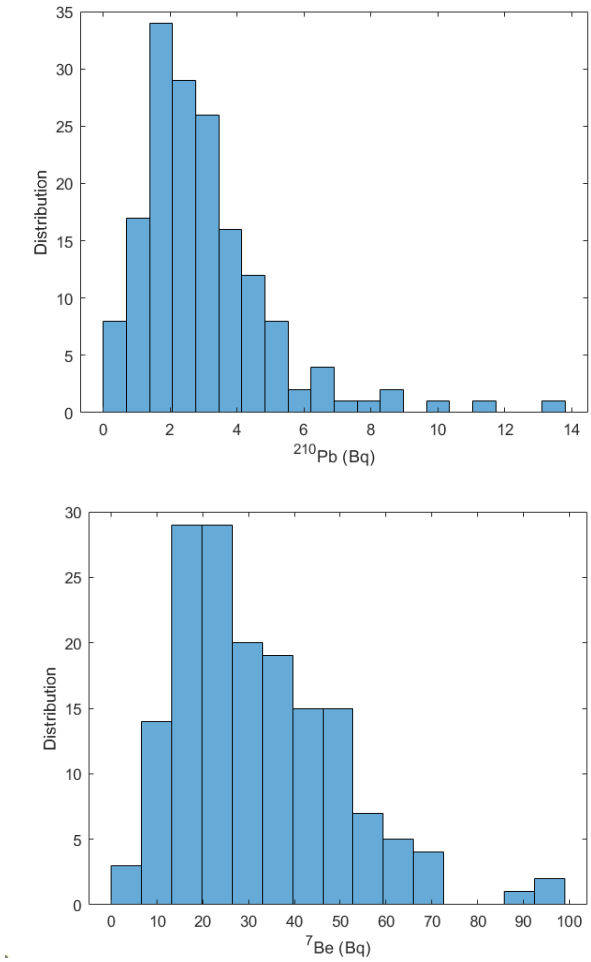

Figure 3.3: Histograms of both ^{210}Pb (top) and ^{7}Be (bottom), showing the distribution of activity measurements of each nuclide across the entire data set.

3.2.2 Sample Volume Data

In addition to the gamma ray counting data, data logs for the start date, stop date, date of filter collection, total air sample volume in m^3 and air flow rate in m^3/hour were collected for each air filter, as part of participation in the US EPA's RADNET program. These data are used to evaluate data points in the plots above as possible outliers due to reasons such as unusually long or short air sampling times or volumes.

For example: The large activities detected on February 12, 2016 are from a normal sample run, and are therefore not an artifact of increased sample volume. The air filter collected December 1st, 2016 is collected early, sample volume of 4521.1 m^3, and the sample from October 12, 2016 has a sample volume of 8323.6 m^3 due to a power failure during the sampling run, likely due to a windstorm. The sample with end date June 23, 2016 has a low sample volume of 3244.9 m^3, but ran for the full 200 hours. Since the gamma counting data is consistent with the data before and after it, the June 23 data point is not omitted.

3.2.3 Monthly Averaged Activity Data

The following were carried out on the full data set: the data for each each month in the was averaged (January 2014, February 2014, etc.), to produce a smoother graph of activity over time. The data was also averaged for each month across all years of data collection to produce a plot with a single data point for each month to produce a plot showing overall average activity of each nuclide across one calendar year in the area of Orono, Maine. Figure 3.4 below shows a plot of these monthly averages. The $^{7}Be/^{210}Pb$ ratio has also been calculated for the monthly averages, as changes in the ratio can be an indicator of air mass origin. It is clearly periodic, and has been fitted using a first-order Fourier series fit to better identify the periodicity, giving a period of 11.78 months. In both figures, the error bars are from counting uncertainty, propagated by summation in quadrature. The monthly data shows a better correlation, with $R=0.553$, and $P < 0.00001$.

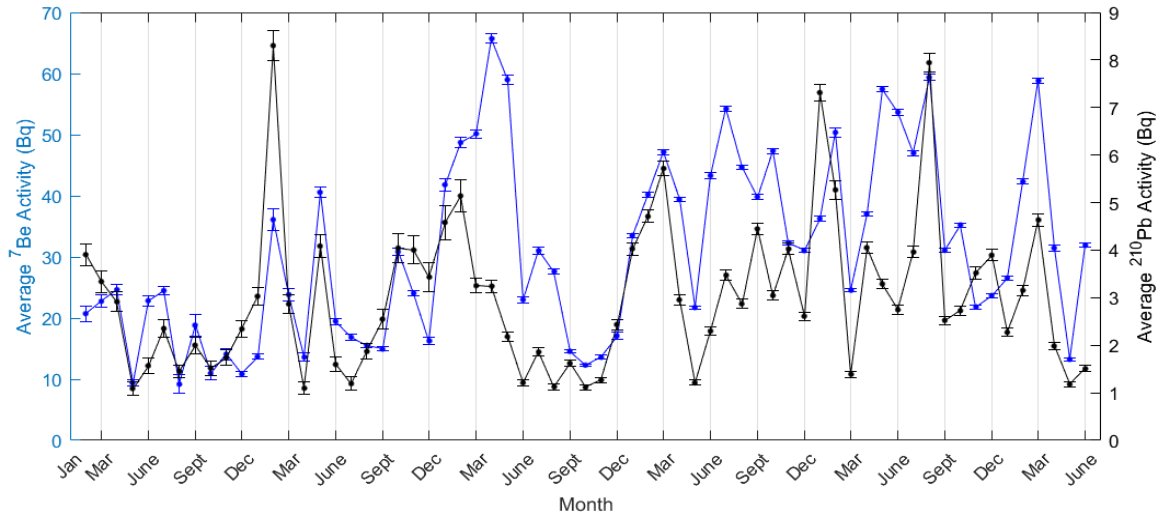

Figure 3.4: The monthly average activity for both nuclides. Error bars represent the error from counting statistics, summed in quadrature.

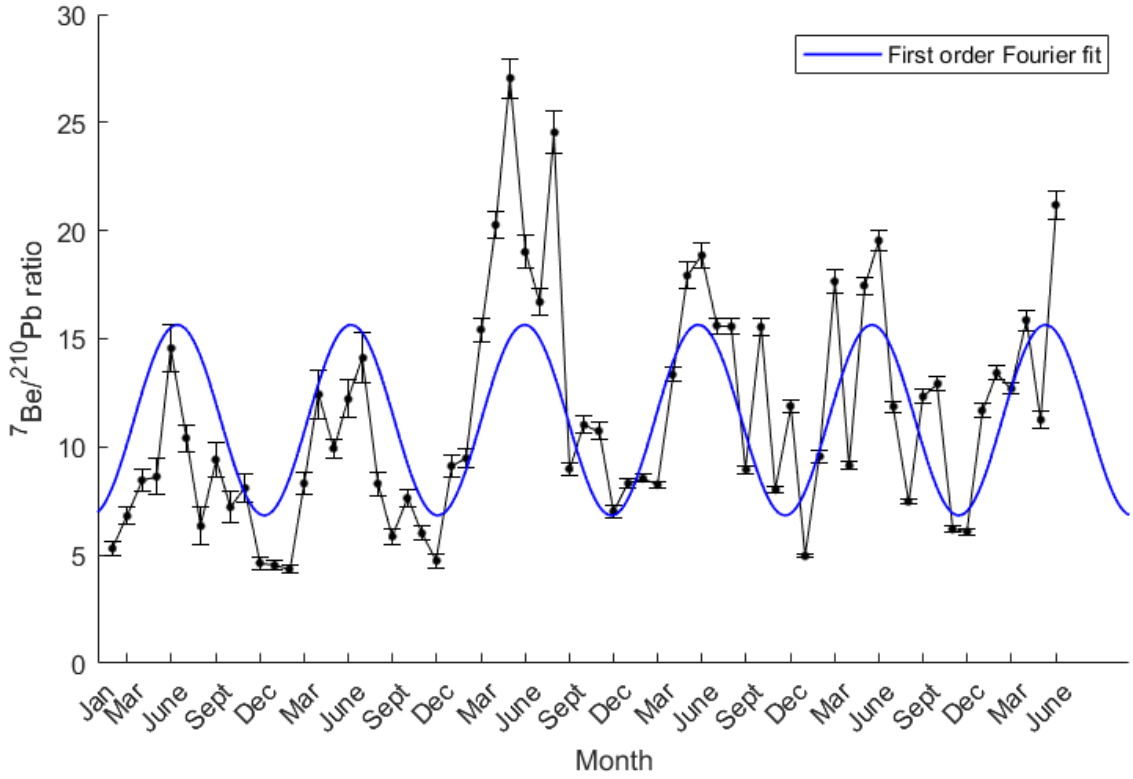

Figure 3.5: Ratio of average ^{7}Be activity to ^{210}Pb activity.

In addition to the $^{7}Be/^{210}Pb$ ratio, the data was plotted with ^{210}Pb and ^{7}Be activities on each axis. To assess seasonality of the data, the points are labeled based on the time of year they represent, with one label for the first and last 90 days of the year, and the other for the middle 180, to identify the colder and warmer months. The resulting plot is shown below, with filled circles for the warmer middle of the year and open circles for the beginning and end of the year.

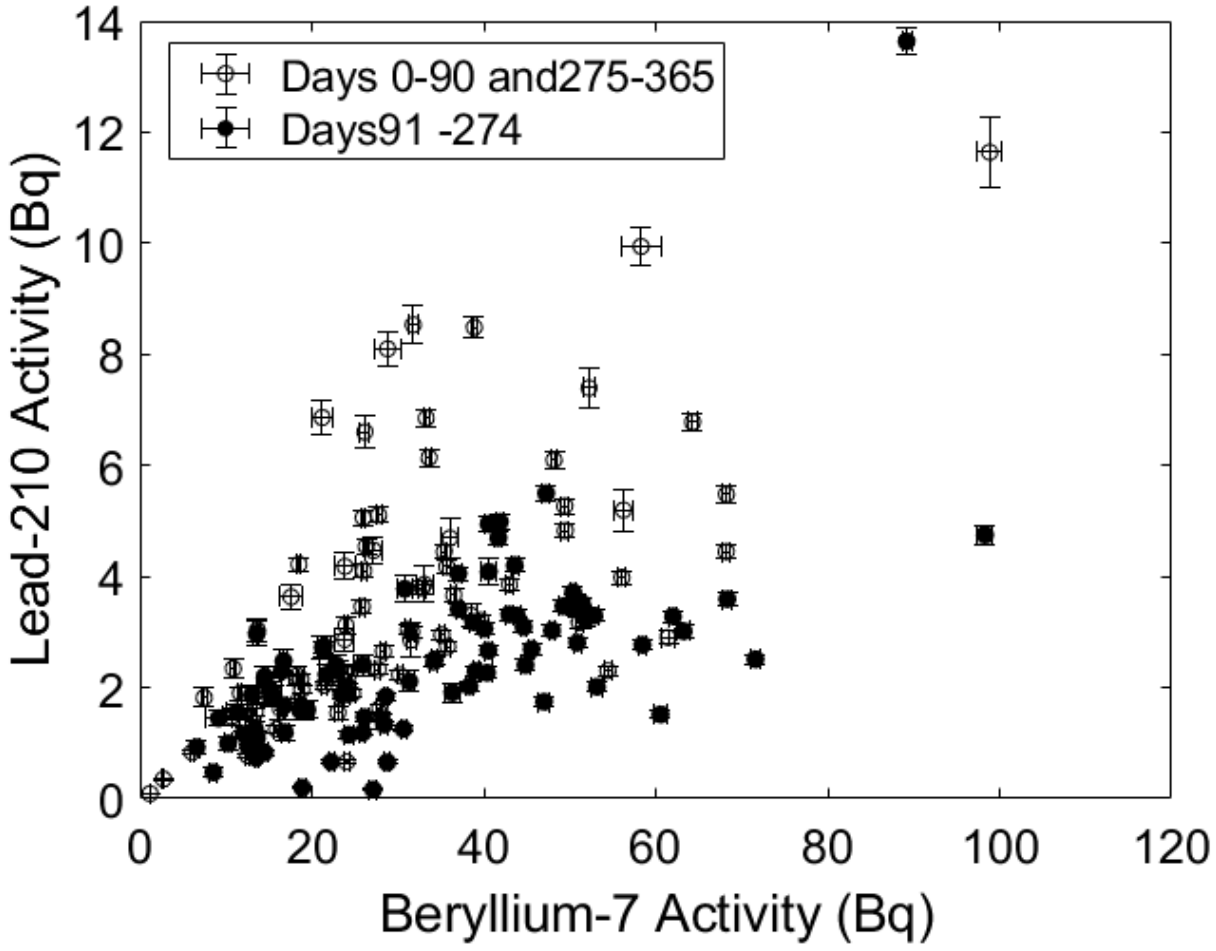

Figure 3.6: ^{7}Be activity plotted against ^{210}Pb activity for Orono, Maine.

The data averaged over the calendar year (i.e. all points for each month are averaged, across years) is tabulated below. The statistical standard deviation of each month's data is also included for each nuclide.

Table 3.6: Averaged data for each calendar month, across all years of data collection.

Month	^{210}Pb activity (Bq)	^{210}Pb standard deviation (Bq)	^{7}Be activity (Bq)	^{7}Be standard deviation (Bq)
January	4.40	2.13	33.2	12.8
February	4.90	2.88	38.2	21.9
March	3.56	1.68	39.5	17.4
April	2.80	1.08	38.7	17.4
May	1.79	1.07	30.7	20.9
June	1.91	0.91	34.9	17.5
July	2.56	0.95	37.2	16.7
August	3.38	3.32	38.3	19.6
September	2.71	1.19	24.0	11.3
October	2.56	1.66	28.5	16.7
November	2.98	2.14	21.4	9.9
December	2.96	1.68	20.9	10.5

Note that some months have particularly high standard deviations for either ^{210}Pb, ^{7}Be, or both nuclides, suggesting that those months contain statistical outliers within their data sets. February has large standard deviations for both nuclides, due to unusually high activities for both occurring on February 12, 2016 of 11.6 and 98.8 Bq, respectively; and a second high value for ^{7}Be on February 24, 2017, of 68.2 Bq. May shows a large standard deviation for ^{7}Be only due to the following activity values: 6.61, 13.0, and 8.55 Bq in May 2014; 16.8 and 13.5 Bq in May 2017; and 13.2 Bq in May 2019. August has a very large standard deviation for ^{210}Pb due to the following: very small activities of 0.196 and 0.164 Bq on August 3 and 12, 2016, and an unusually large activity of 13.6 Bq on August 10, 2018. The ^{7}Be standard deviation for August is large, due primarily to an activity of 89.1 Bq on August 10, 2018. The data for August 2016 are lower, but not as anomalous as those for ^{210}Pb on the same dates. ^{210}Pb has another high standard deviation for November, due to a high value of 7.39 Bq on November 15, 2015, and two low values of 0.774 and 0.834 Bq occurring on November 4 and 28, 2016.

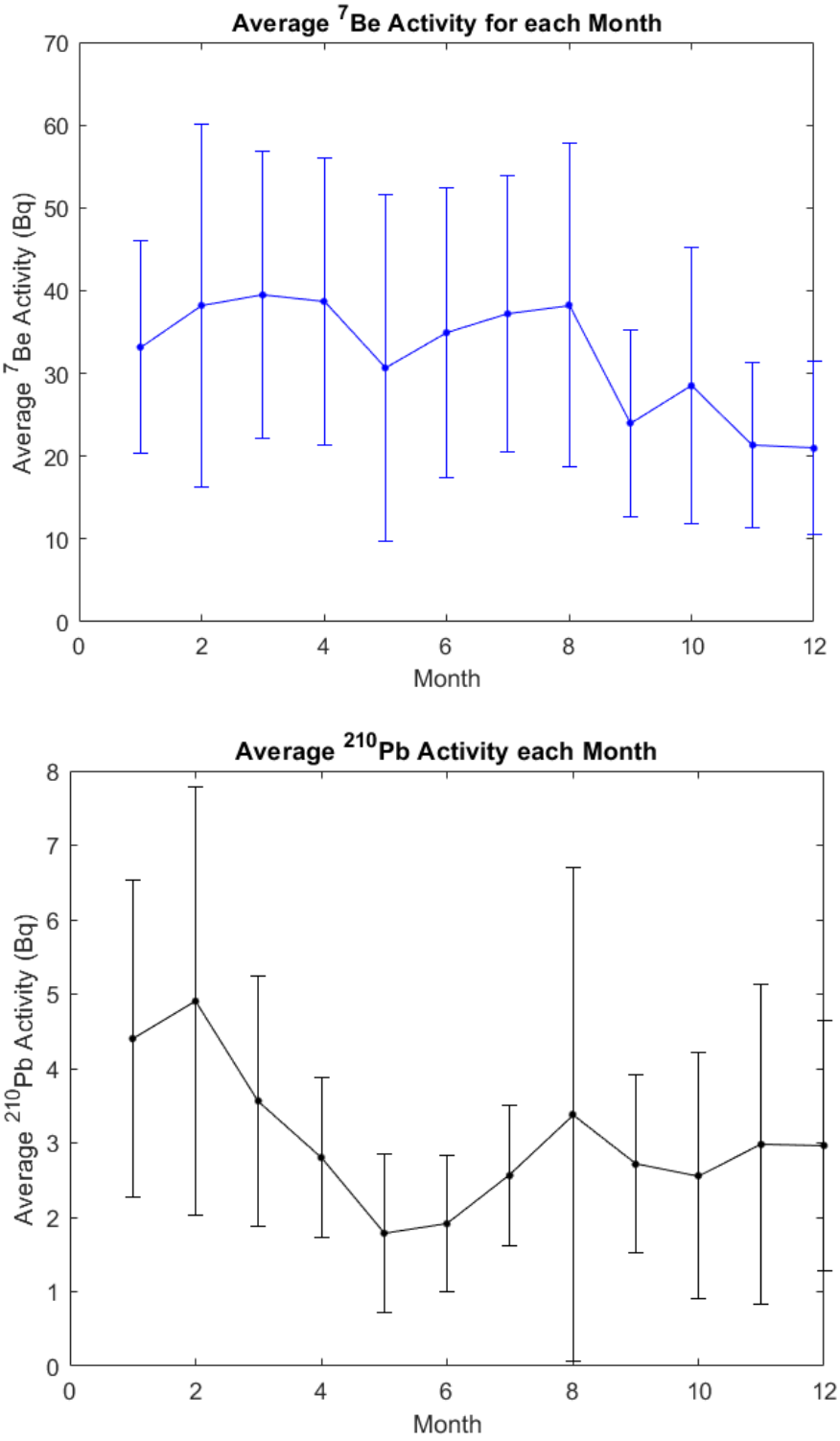

Figures 3.7 and 3.8: Monthly activity averaged for all data points from each year's data, for ^{7}Be and ^{210}Pb, respectively. The error bars represent the standard deviation of each point.

3.3 Air Filter Collection Efficiency Data

Several runs of two filters stacked on top of each other were taken, to check the efficiency of the air filters in collecting radioactive material from the air. The filters used in the EPA RADNET air sampler have an efficiency of greater than 97% for particles of sizes 0.2 μm or larger (US EPA, personal communication). The efficiency of the counting system has already been considered, but if one were to generalize to the total activity in the air, the efficiency of the filters would also need to be known. If a large portion of material passing through the filter is not trapped within it, it would not produce a truly accurate measurement.

For each pair of stacked filters, each filter was counted separately for the same time interval, and the efficiency of an air filter estimated by $\alpha = 1 - \frac{bottom\ filter\ counts}{top\ filter\ counts}$, with α being the efficiency for the nuclide in question. It should be noted that, since the bottom filter has relatively low total counts, the uncertainty from counting statistics will be high. The uncertainties in efficiency for each individual run were calculated by summation in quadrature of the uncertainty of the counting uncertainty of the counts for each filter used in the equation above. The uncertainty from counting statistics is calculated as (peak gross counts+subtracted background counts)$^{1/2}$.

The average efficiencies are 0.748 for ^{210}Pb and 0.746 for ^{7}Be. The efficiencies as calculated above are smaller than the efficiency for the filters, suggesting either that the model used in calculating efficiency is incorrect, or that some of the airborne radioactivity is on particles smaller than 0.2 μm. The assumptions made in the model also do not account for factors such as the first filter collecting a majority of the large airborne particles, which could lead to the second filter collecting a proportionally smaller amount of material because only smaller particles, where the filters are less efficient, will pass on to it.

Table 3.7: ^{210}Pb data for pairs of filters and resulting efficiencies.

Date Collected	Background- Subtracted Net Counts		Efficiency	Efficiency Uncertainty (%)
	First	Second		
06/03/2016	323.5	54.5	0.832	77.9
07/02/2016	201	62	0.692	70.2
11/17/2016	261.5	154.5	0.409	34.3
12/17/2016	653	197	0.698	24.0
01/18/2017	1168	231	0.803	20.2
02/24/2017	813	213	0.738	22.5
03/28/2017	1268	226	0.822	19.6
04/20/2017	846	116	0.863	34.6
07/06/2017	932	115	0.876	35.9

Table 3.8: ^{7}Be data for pairs of filters and resulting efficiencies.

Date Collected	Net Counts		Efficiency	Efficiency Uncertainty (%)
	First	Second		
06/03/2016	2119.5	292.5	0.862	10.1
07/02/2016	2948.5	784	0.735	5.17
11/17/2016	2075.5	1291.5	0.377	4.40
12/17/2017	3047.5	978	0.679	4.83
01/18/2017	11019	2396.5	0.782	2.62
02/24/2017	1438.5	3259.5	0.772	2.23
03/28/2017	15285.5	2496.5	0.837	2.51
04/20/2017	9266	1582	0.829	3.48
07/06/2017	12844.5	2023.5	0.842	2.89

3.4 Mass collected by air filters data

From late September, 2015 to the end of November 2017, data was collected to study the effect the collected mass of material might have on the radioactivity detected on each filter after an air sampling run. Each air filter was massed before it was used, and again after, and the data tabulated. The difference between the initial and final air filter mass is treated as the mass collected on the filter during the air sampling run. In the cases where two filters were run, only the filter on top of the stack is used in the data below, as it will have collected the majority of the material. Table 3.9 below shows an example of the data, with the full data available in an appendix. The collected mass is found by subtracting the initial filter mass from the mass after an air sampling run.

Table 3.9: Example data for filter mass before and after air sampling

Date filter was collected	Initial mass (g)	Mass after sampling (g)	Collected mass (g)
09/28/2015	4.2060	4.3289	0.1229
10/06/2015	4.3656	4.4424	0.0768
10/15/2015	3.9008	3.9981	0.0973
10/24/2015	3.9490	4.0545	0.1055
11/04/2015	3.9447	4.0272	0.0825
03/26/2017	4.2906	4.3732	0.1826
04/03/2017	4.2409	4.3571	0.1162
04/12/2017	4.0082	4.2977	0.2895

Figure 3.8 shows the data, plotted over time. Note that there is an obvious outlier in the data with a collected mass of 0.5632 g, occurring at t = 630 days, on June 19, 2017. The average initial filter mass is 4.0752 g, with a standard deviation of ±0.2320 g. The average collected mass is 0.1426 g, with a standard deviation of ±0.08246 g. Since an outlier occurs in the mass data at t=630 days, omitting this outlier point in the sample mass data gives an average of 0.1366 g for the collected filter mass, and a standard deviation of ±0.06555 g.

The filter mass data over time has also been fitted using a first-order Fourier series fit of the form $Y = A + B*\cos(\omega t) + C*\sin(\omega t)$. Figure 3.9 shows the data plotted along with the fitted function. The angular frequency of the fit is 0.01554 radian/day, corresponding to a period of 404 days. The Pearson correlation coefficients between the collected mass and both the ^{7}Be and ^{210}Pb activity have been calculated using Matlab's corrcoef function, giving R = 0.2790 and R = 0.2356 for ^{7}Be and ^{210}Pb, respectively. Therefore, the sample mass does not have a strong correlation to either measured activity, and is unlikely to be one of the major influencing factors, even though it also varies over time.

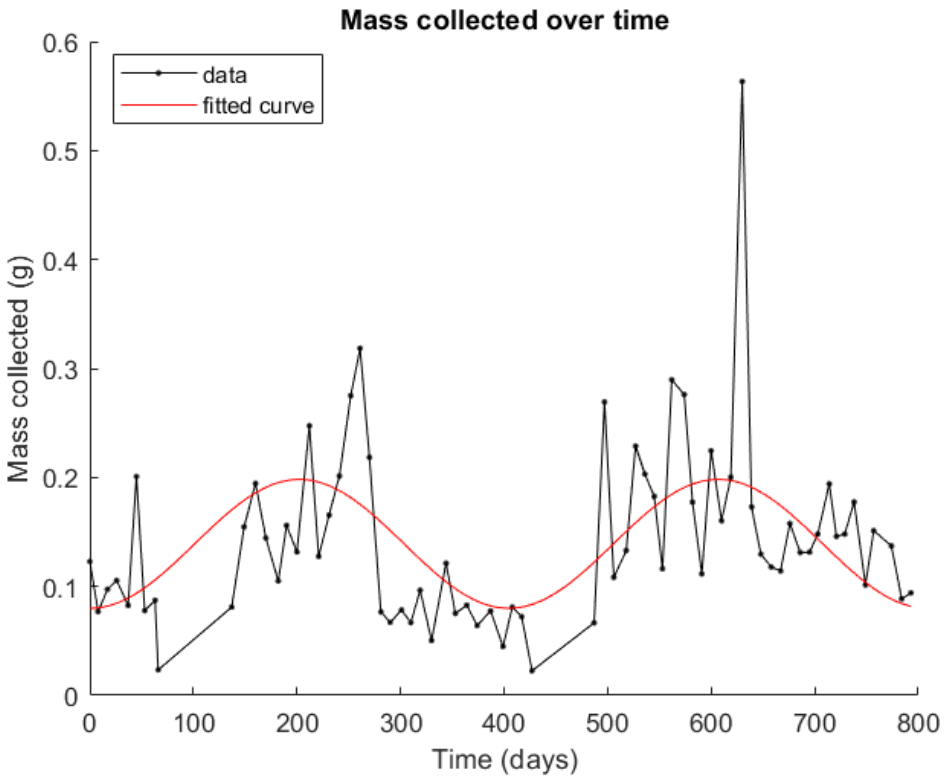

Figure 3.9: Mass collected over time with first-order Fourier series fit. T = 0 corresponds to a date of September 28, 2015, and the end of the data at t = 793 corresponds to a date of November 29, 2017.

3.5 Examination of Airborne Nuclide Activity and Weather Data

Data for precipitation and snowfall were collected from the NOAA National Centers for Environmental Information, in the form of GCHN-Daily data for the duration of the data collection period for the air sampling (NOAA National Centers for Environmental Information, retrieved 02/09/2022). The Bangor International Airport weather station was chosen for its proximity to the University of Maine and completeness of the data available.

The total precipitation for the eight days of each sampling period was calculated by summing the precipitation data and snowfall data over each period separately. Then, to estimate the water equivalent of snow, the snowfall is divided by ten and added to the precipitation. It is this result of total precipitation plus estimated water-equivalent of snow that is plotted below. Figures 3.10 and 3.11 show the precipitation and activity data for ^{210}Pb and ^{7}Be, plotted over the entire time of the experiment.

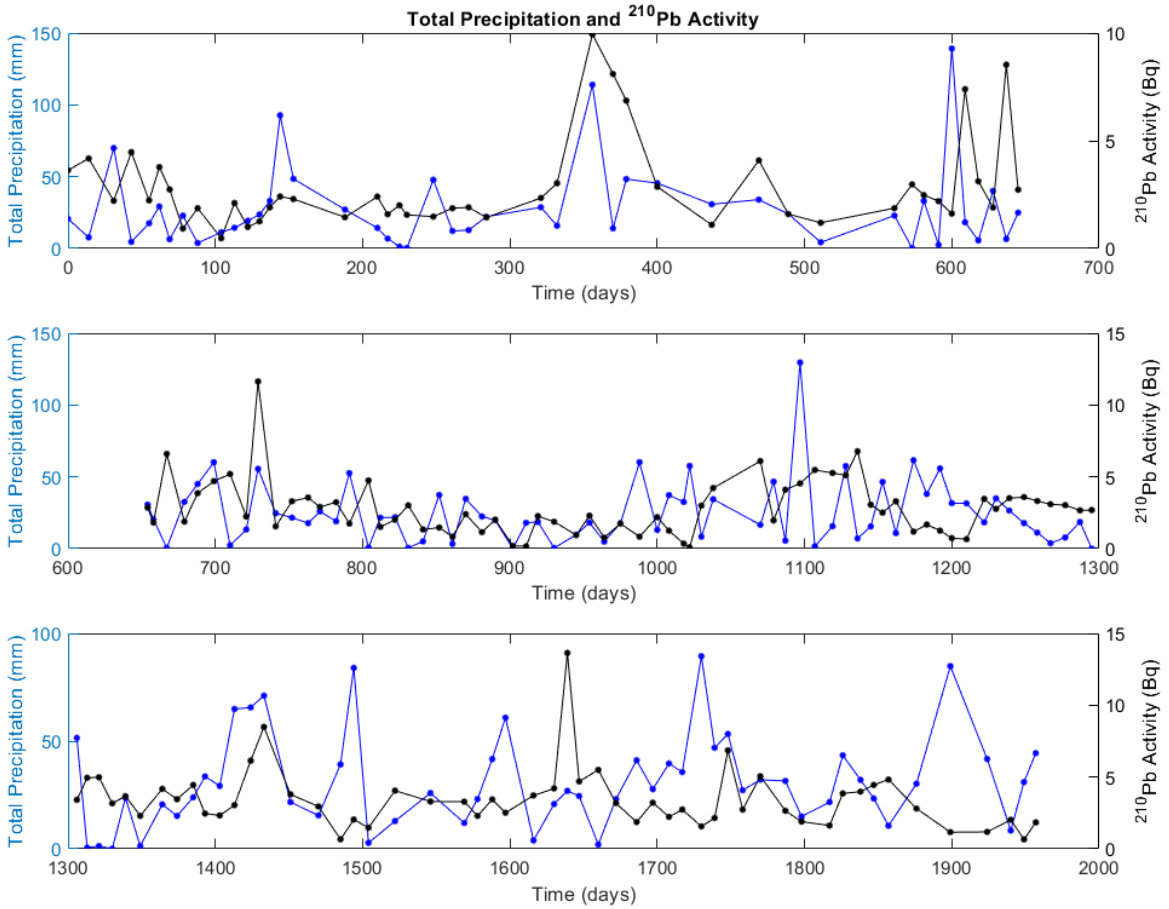

Figure 3.10: Precipitation and ^{210}Pb activity over time. The beginning and end points for the data are the same as for the full time series activity data, February 13, 2014 to June 24, 2019. Precipitation is plotted in blue, and ^{210}Pb activity is plotted in black. For ease of reading, the plot has been split roughly into thirds.

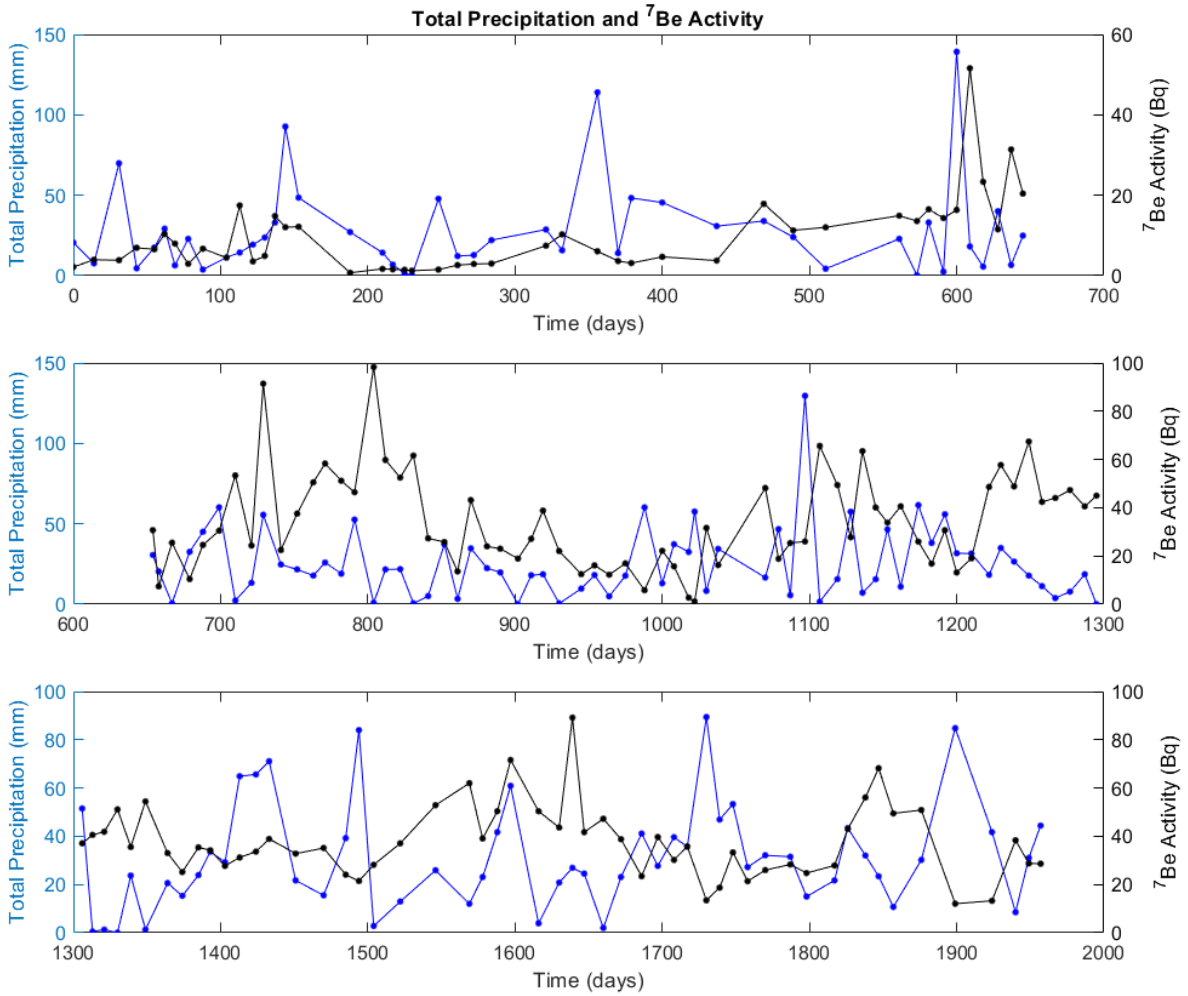

Figure 3.11: Precipitation and ^{7}Be activity over time. Same beginning and end points as Fig. 3.10 above. Precipitation is plotted in blue, and ^{7}Be activity is plotted in black.

The Pearson correlation coefficients from Matlab's corrcoef function between the precipitation and each nuclide's activity data are as follows: for ^{210}Pb, R = 0.0538, and P = 0.4949; and for ^{7}Be, R= -0.1365, and P = 0.0823. The P values represent a significance of the correlation coefficients. If they are below the significance level (by default, 5%, or 0.05, corresponding to a confidence interval of 95%), then the correlation can be considered significant. By visual inspection, there are clearly isolated

areas in time where high precipitation corresponds to lower radioisotopes present, and vice-versa, but there is no clear and consistent trend.

If, instead, total monthly precipitation and monthly average values for each nuclide activity are considered, the correlation coefficients are -0.1584 for ^{210}Pb and 0.1737 for ^{7}Be. The P values are 0.1665 and 0.2076, respectively. Visual inspection, however, does show clear regions in time where large total precipitation corresponds to lower values of activity for both nuclides. Plots of these monthly aggregate data are shown in the figures below.

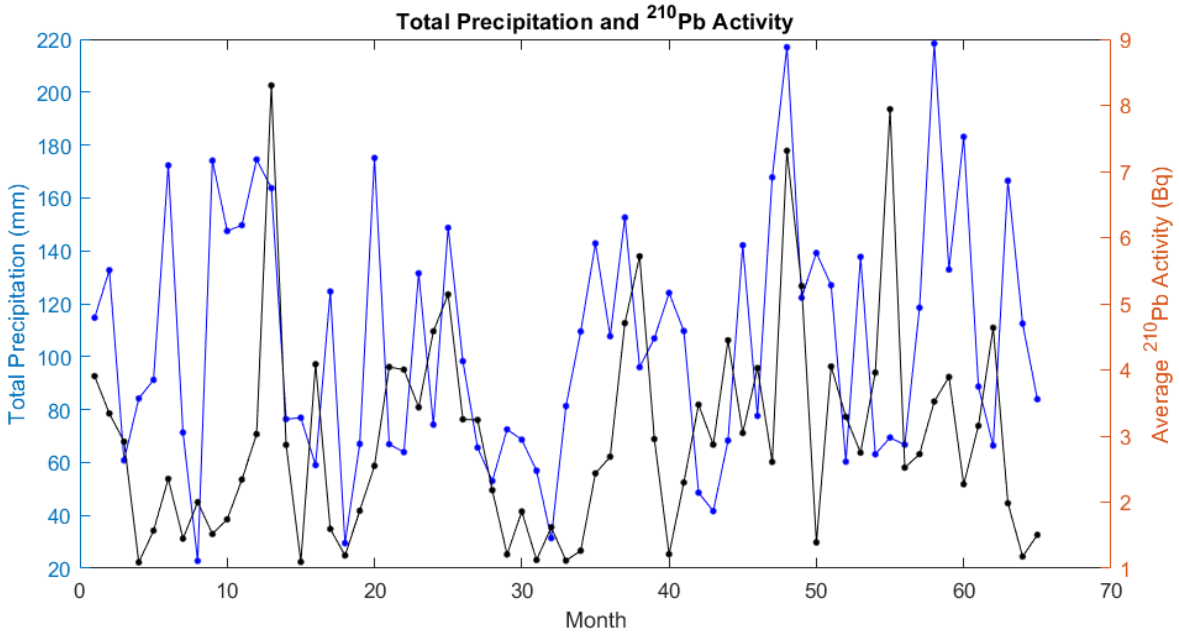

Figure 3.12: Monthly total precipitation and average ^{210}Pb activity. The data begins with February, 2014 as month 1, and ends with June, 2019 as month 65.

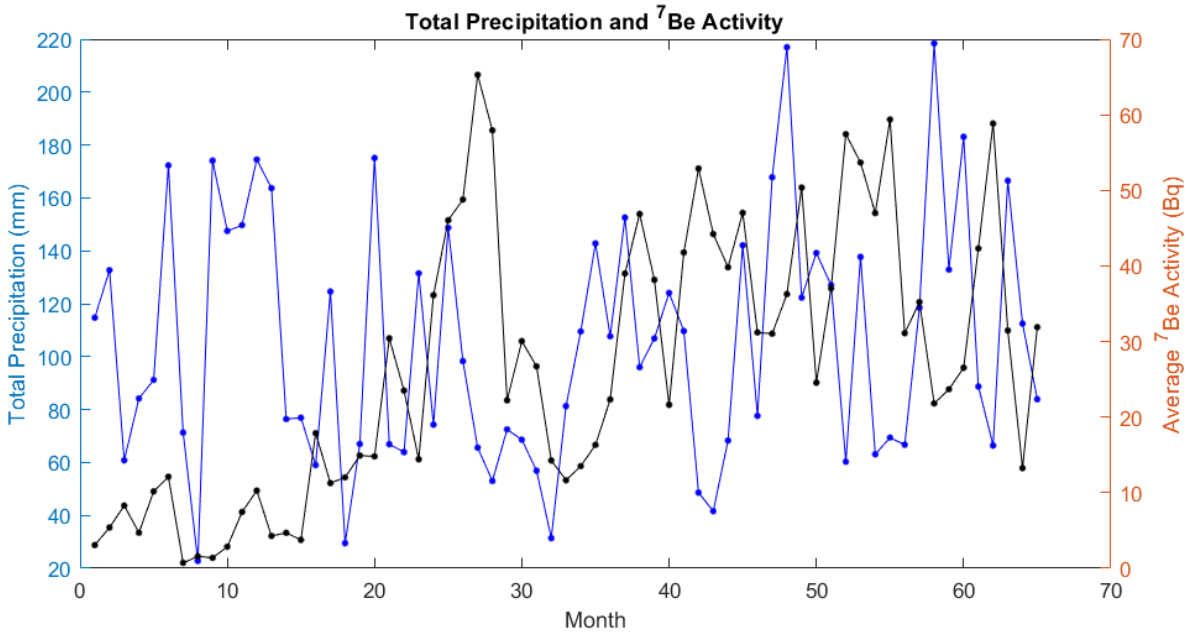

Figure 3.13: Monthly total precipitation and average ^{7}Be activity. The data start and end points are the same as in figure 3.12 above.

CHAPTER 4

DISCUSSION OF RESULTS

4.1 Summary of Results

The overall average value for ^{210}Pb activity across the entire data set is 3.029 Bq, with a standard deviation of ±2.05 Bq. The range for ^{210}Pb activities is 0.0907 to 13.64 Bq. The distribution for activity values is lognormal, and shows a peak in the distribution of activities in the range of 1.5-2.5 Bq. The overall average for ^{7}Be across the data set is 32.13 Bq, with a standard deviation of ±17.9 Bq. The range for ^{7}Be is from 1.18 to 98.8 Bq. The distribution is roughly lognormal, with a peak in the distribution around the 10-25 Bq range, and a broader overall shape. The Pearson correlation coefficient, as calculated by Matlab, between the lead and beryllium activities, is 0.5932, with a p-value of $7.22*10^{-17}$, much smaller than the significance level of 0.05, suggesting that the correlation between the two nuclide activities is significant.

The average efficiency for the air filters used, as calculated by radioactive counting, is 74.6% from the ^{7}Be data and 74.8% from the ^{210}Pb data. The uncertainties on the ^{210}Pb data are quite large due to overall lower count rates, and a subtraction of an additional background peak from the lead shield around the detector. The ^{7}Be data have much smaller uncertainties from counting statistics.

The mass collected on the air filters has an average of 0.1366 g, with a standard deviation of ±0.06555 g. The average and standard deviation are both calculated after omitting a large outlier data point visible in the plotted data. The collected mass varies over time in a periodic fashion. There is no clear correlation between the mass collected by the air filters and the activity of either radionuclide.

A comparison between the measured radionuclide activities and total precipitation in the area shows a similar lack of clear correlation overall. However, there are clear times where high amounts of precipitation are associated with low activities of both ^{7}Be and ^{210}Pb, suggesting that there is some washout effect.

4.2 Discussion of Results

The efficiency of the filters, according to the measured radioactivity in one filter compared to one directly below it, is around 75% for both radionuclides. Due to the counts on the second filter often being close to the background, the uncertainty from counting statistics is very high for the ^{210}Pb, leading to large net uncertainties in the calculated efficiencies. Since it produces a much larger peak and has no presence in the background spectra, the ^{7}Be data has much lower uncertainty overall, and is therefore a better nuclide for analysis with such a method. That the two radionuclides are on average in good agreement is not surprising, since both nuclides are carried in suspended aerosols. The efficiencies found by this experimental method are much lower than those reported by the EPA, (75% total versus >97% for particles larger than 0.2 microns). This is likely due to the model I used in calculating the efficiency not taking aerosol particle size into account, and simply looking at the total radioactivity as some evenly-distributed concentration that is pulled out of the air at some rate by the air filter.

Since the first filter should collect a large proportion of suspended aerosols above 0.2 microns in size, the amount of material the second filter can collect is significantly reduced. However, in the case of ^{7}Be, the second filter still often had easily resolvable peaks of several thousand counts in a 12 hour counting period, suggesting that a fair amount of airborne radionuclides are on particles smaller than 0.2 microns, or otherwise pass through a single air filter and will not be detected.

Since the efficiencies I calculated for the air filters are roughly 75%, it is possible that the activities measured in my study do not reflect the true activities or concentrations in the sampled air. For comparison within the data set, this presents little issue, as the same air sampling system and type of air filter was used for the entire experiment. There may, however, be some issues in comparing my data to other data collected with different systems.

The general behavior for monthly averaged values of ^{7}Be, as seen in Fig. 3.4, follows a pattern of increases over winter, a drop somewhere in early spring followed by increasing over the summer and dropping again in the fall, to repeat the slow increase over the winter. For the most part, the ^{210}Pb monthly averages follow a similar pattern, although the increases in the spring and summer are often smaller, and there are isolated periods of anticorrelation between the two radionuclides, such as summer in 2018. When the data is instead averaged over all years for each month, as in Figs. 3.4 and 3.5, the ^{7}Be activity is relatively flat, until it declines in the fall, and the ^{210}Pb activity is high at the beginning of the year, drops to a low around June, and then is relatively flat for the rest of the year. The averages taken of all data for each month have relatively high standard deviations, suggesting a large amount of variance in the data.

In the case of the data averaged for each month across all years, the standard deviations for each month are relatively high, and in some cases, clear outliers are present in the data. The plot of ^{7}Be data suggests a fairly flat amount of ^{7}Be on average, instead of an expected curve with an increase in warmer months, as the data plotted for each month of data collection might suggest. The ^{210}Pb plot for each month suggests a lower amount of ^{210}Pb in the summer. The high standard deviations for these graphs suggest that the data is, on average over the course of a year, relatively flat for each radionuclide. It may be safe to conclude that, particularly in the case of a long-lived isotope like ^{210}Pb, that the amount of ^{210}Pb is roughly constant year-round.

While there is a clear correlation between the activities of ^{7}Be and ^{210}Pb collected in air sampling, there are no strong correlations between either radionuclide and the mass of material collected on the air filters or the amount of precipitation. That there are still occasions where high precipitation corresponds to low radionuclide activities or vice-versa, it does still suggest that some washout effect occurs.

The $^{7}Be/^{210}Pb$ ratio is consistently higher in the spring and summer, and reaches a low in fall and winter. The plot of ^{7}Be against ^{210}Pb also shows a clear seasonality, with a larger scattering among the points in the cooler parts of the year. Comparatively, the warmer months tend to have lower values of ^{210}Pb and cluster within the lower portion of the plotted data. The ratio between these two radionuclides can be an indicator of air mass origins. Since very little ^{222}Rn is released by the ocean, ^{210}Pb is primarily released over the continents and the concentration of ^{210}Pb is higher in air originating over continental landmasses (Baskaran et. al, 1993). The concentration of ^{7}Be in the atmosphere, due to its cosmogenic origins, is not dependent on the origin of a given air mass. Therefore, a higher ratio of ^{7}Be to ^{210}Pb may suggest air of oceanic origin. It is reasonable to conclude that in the spring and summer months, Maine receives more air of oceanic origin than of continental origin. However, an alternative explanation is that these periods experience a greater degree of mixing between the troposphere and stratosphere, leading to more transport of ^{7}Be into the lower atmosphere.

Shown in the figures below are climate reanalysis maps for the United States, showing the average wind speed and direction at 10 meters for each season in 2016. The maps were produced using the Climate Reanalyzer website, using the ECMWF ERA5 reanalysis model. The trends in these plots are typical for all years airborne radionuclide data was collected. In the winter, the average air flow toward Maine is from the West and Southwest, originating across the continent. In spring, continental air flows from the Northwest, in the summer, the air flows from the Southwest, following the east coast of the US, and in the fall, the air flows are returning to those across the continent seen in winter. While it is possible that the wind patterns indicate dominance of continental air in the winter and oceanic air in the summer, this observation is qualitative only, and competing with other explanations of the same phenomenon. Further research using a more detailed approach to air mass origin, for example, via back-trajectory analysis of air flows during the sampling period, to better show any effects of oceanic versus continental air on radionuclide activities.

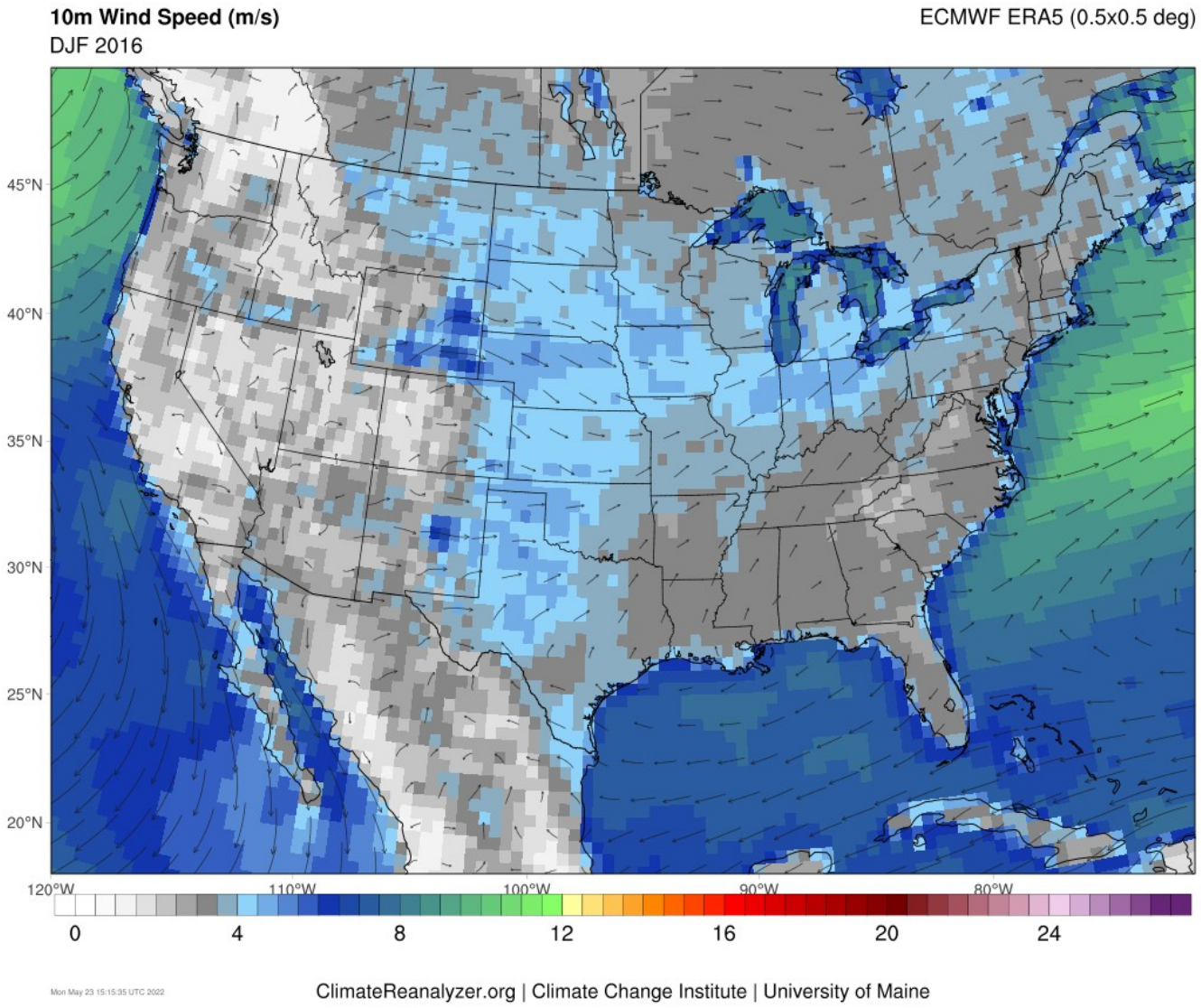

Figure 4.1: Climate reanalysis map for the USA, showing average 10m wind vectors during December 2015 and January and February 2016 (Climate Change Institute, Hersbach et al., 2019).

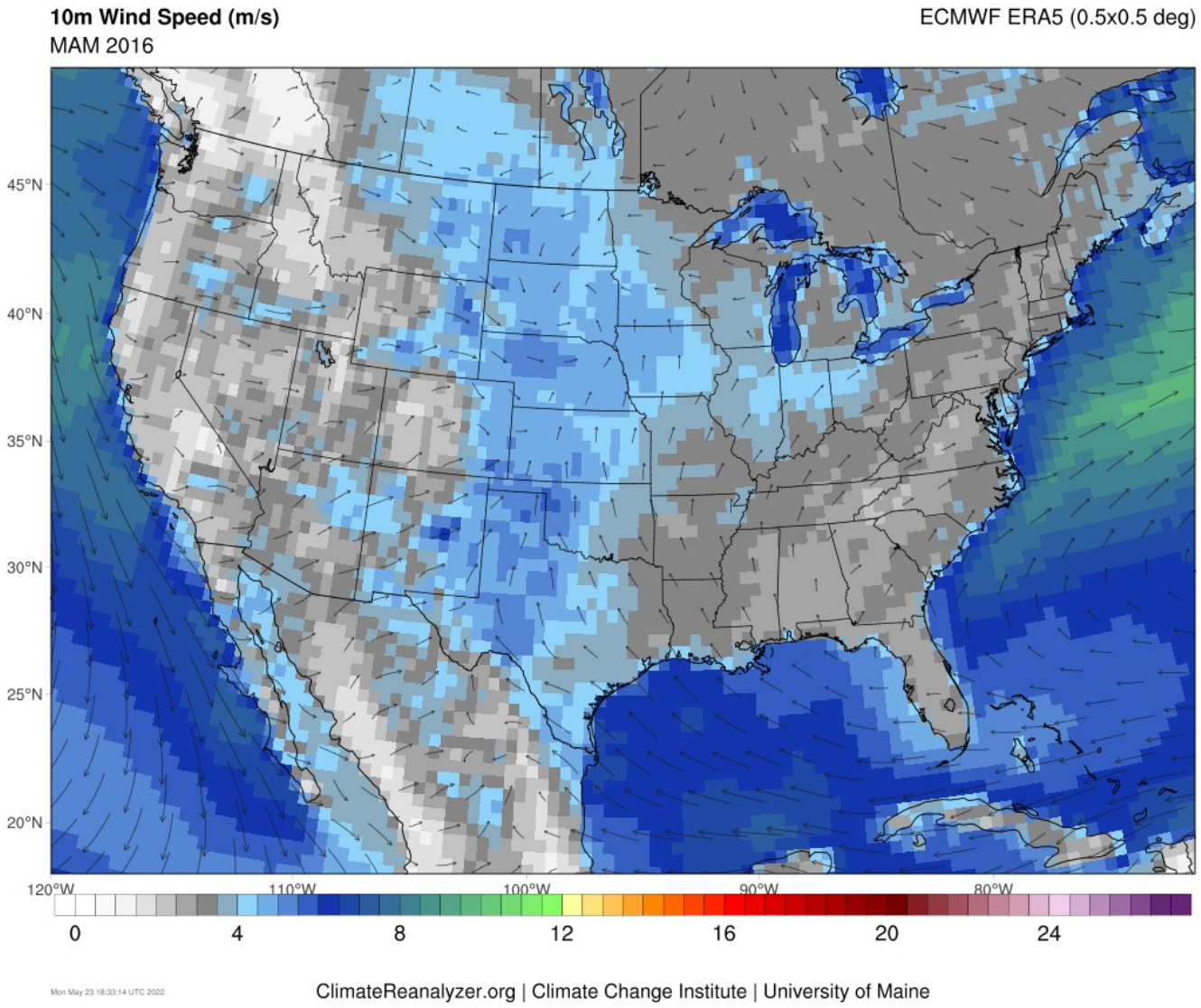

Figure 4.2: Climate reanalysis map for the USA, showing average 10m wind vectors during March, April and May 2016 (Climate Change Institute, Hersbach et al., 2019)

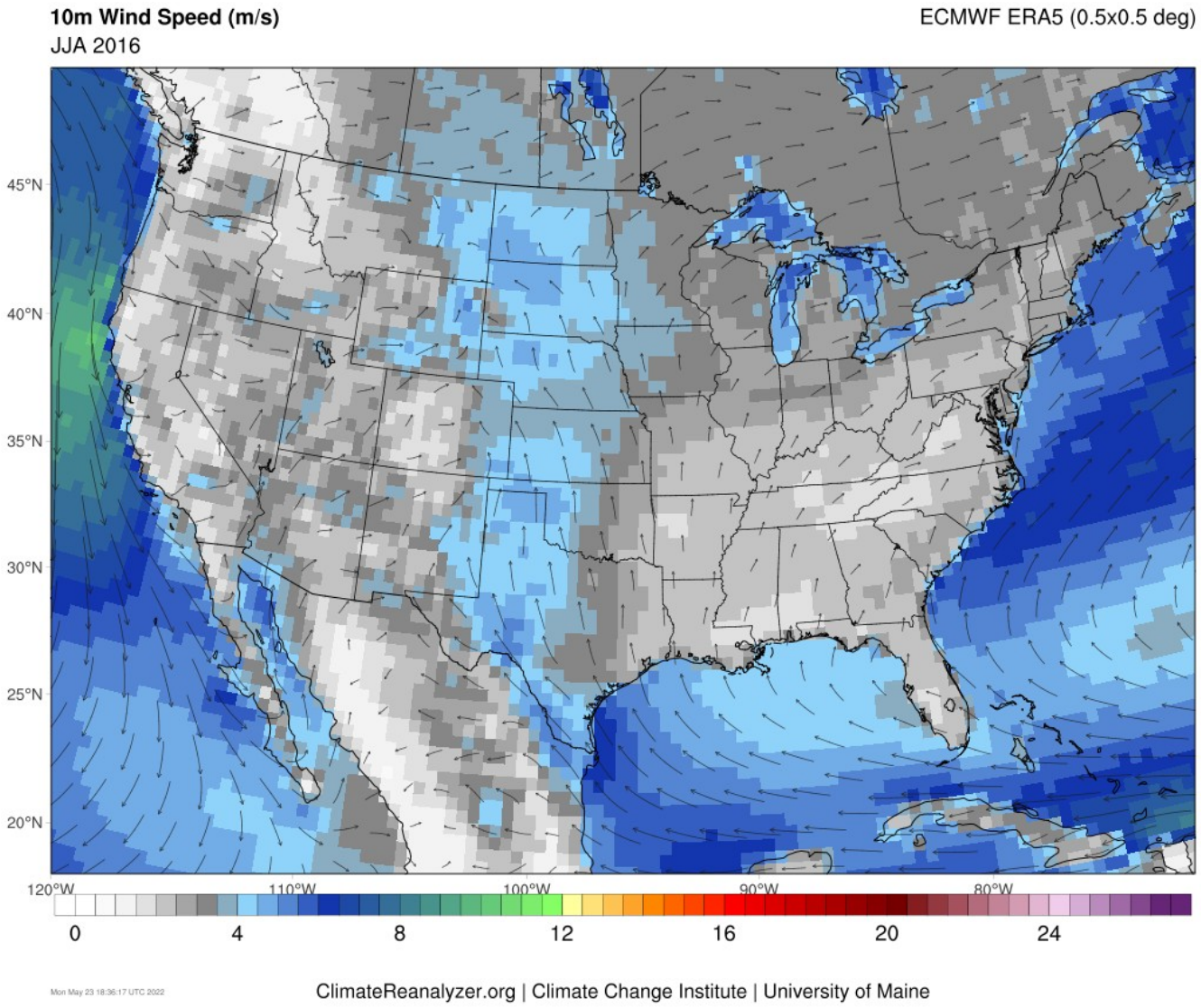

Figure 4.3: Climate reanalysis map for the USA, showing average 10m wind vectors during June, July, and August 2016 (Climate Change Institute, Hersbach et al., 2019).

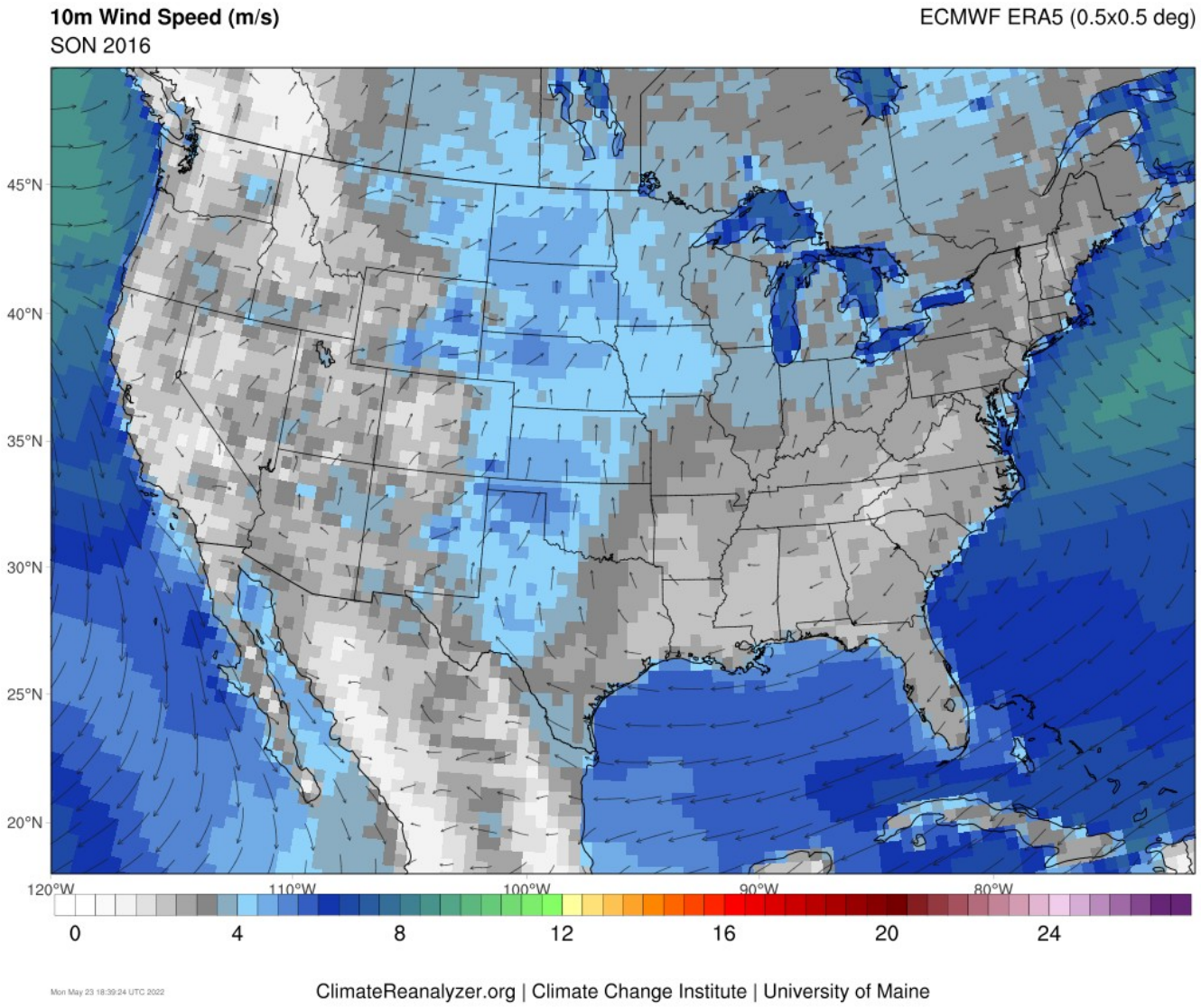

Figure 4.4: Climate reanalysis map for the USA, showing average 10m wind vectors during September, October, and November 2016 (Climate Change Institute, Hersbach et al., 2019).

4.3 Comparison with literature results

The range of values for each nuclide are 0.0907 to 13.64 Bq for ^{210}Pb and 1.178 to 98.8 Bq for ^{7}Be. The arithmetic means for each data set are 3.029 Bq and 32.13 Bq for ^{210}Pb and ^{7}Be, respectively. In the literature, the activity concentration is considered instead of the absolute activities of each nuclide. For ease of comparison, the above values are converted into concentrations using the average sample volume of 12000 m^3, giving the following values: 7.56 µBq m^{-3} to 1.13 mBq m^{-3} with an average value of 0.252 mBq m^{-3} for ^{210}Pb, and 98.2 µBq m^{-3} to 8.23 mBq m^{-3} with an average of 2.68 mBq m^{-3} for ^{7}Be. The average results are consistent with results from Edinburgh, 0.21±0.01 and 2.50±0.04 mBq m^{-3} (Likuku, 2006), but are not consistent with the results from Greece, 664 µBq m^{-3} and 5.03 mBq m^{-3} (Ioannidou et al., 2005) or Spain, 0.54 mBq m^{-3} and 4.6 mBq m^{-3} (Dueñas et al., 2011), being roughly half as large as the literature values.

The results for ^{210}Pb are not consistent with those from Belgrade (0.109 to 3.09 mBq m^{-3}) (Todorovic et al., 2005), with my values showing much smaller minimum and maximum values. Nor are my results consistent with those from Edinburgh (0.01 to 0.74 mBq m^{-3}), showing a higher maximum value despite the similar mean. My results are consistent with those from Greece (0.108-1.982 mBq m^{-3}), France (0.34-1.35 mBq m^{-3}) (Bourcier et al., 2011), and Spain (0.24-1.40 mBq m^{-3}), although the minimum value in my data is much lower.

The results for range of ^{7}Be show a minimum value an order of magnitude smaller than those in the literature, in all cases. The maximum value of 8.19 mBq m^{-3} is not consistent with those from Belgrade (18.3 mBq m^{-3}) and Greece (12.70 mBq m^{-3}), but is consistent with those from France (7.73 mBq m^{-3}) and Edinburgh (6.54 mBq m^{-3}).

Qualitatively, my data shows a similar seasonal variation as that observed in the literature. The local maxima in the winter for both radionuclides in my data may be due to large-scale influences such as the circulation of air from polar regions toward Maine during the winter months. Polar air would be enriched in ^{7}Be due to a higher rate of production nearer to the geomagnetic poles, and also enriched in ^{210}Pb from passage primarily over the North American continent before its arrival.

My results for a correlation between precipitation and radionuclide concentration suggest a weak or no correlation overall between precipitation and either radionuclide's activity. This conclusion is in agreement with Ioannidou et al., who also show no correlation between either ^{210}Pb or ^{7}Be and rainfall amount, but do note that isolated cases of very high precipitation result in low concentrations of both nuclides. Likuku also shows that precipitation has an influence on both nuclide concentrations, but it is not the only contributor to variation in those concentrations. My correlation coefficient between ^{7}Be and ^{210}Pb activities is 0.553 for the monthly activities and 0.59 for the entire data set. This is consistent with the results from Greece (0.62, $p < 0.0001$) (Ioannidou et al., 2005). The seasonal variation of the ^{7}Be/^{210}Pb ratio is consistent with those seen in the literature, showing high values in the spring and summer and low values in fall or winter. While the most likely explanation is increased vertical mixing, it is also possible that changes in wind patterns lead to circulation of oceanic air masses with reduced ^{210}Pb content, as seen at Stony Brook (Renfro et al., 2012).

CHAPTER 5

CONCLUSIONS

5.1 Conclusions

The activities of ^{7}Be and ^{210}Pb collected in air sampling at the University of Maine Orono campus are weakly correlated, with R= 0.593, P<0.00001 for the whole data set, and R= 0.553, P<0.00001 for the monthly average activity values. Therefore, these correlations are significant, but the detected activities themselves do not show a strong, linear relationship. The weaker correlation suggests that some of the time, ^{7}Be and ^{210}Pb activities collected at the University of Maine Orono campus may be independent of each other. This level of correlation is typical of some coastal or oceanic sampling sites (Baskaran et al., 1993). The $^{7}Be/^{210}Pb$ ratio may support this, as it is higher in air of oceanic origin due to the relatively low amounts of ^{210}Pb found in oceanic air (Likuku, 2006, Renfro et al., 2012).

The seasonal variation of ^{7}Be and ^{210}Pb follows a rough pattern of a drop in both values in the spring, followed by high values in the summer months, and low values in the fall, with values usually increasing in the winter, until the next dip the following spring. In the case of ^{210}Pb, the increases in the winter months may be due to air flowing to Maine from across the continent, since continental air is enriched in ^{210}Pb, due to its primary source being the decay of ^{222}Rn exhaled from the soil. The seasonal variation of the $^{7}Be/^{210}Pb$ ratio is consistent with those in the literature, showing peaks in the warmer months during spring and summer, and lows in the fall and winter. Two competing explanations for the variation of this ratio are increased vertical mixing during warmer months, and large-scale air circulation bringing more oceanic air during the spring and summer. Without a more robust analysis of air mass origin at the sampling site during the sampling period, I cannot reach a definitive conclusion that oceanic air arriving at certain times is the primary cause of the variation of the ratio or the overall lower correlation between the two radionuclides.

The mean monthly activities for ^{7}Be are relatively flat, and do not show a notable increase during the spring and summer, although there is a decrease in the fall leading to the end of the year. In the case of ^{210}Pb, the activity values vary from higher in the winter at the start of the year, to a drop in the spring, increasing again in the summer and remaining relatively consistent for the remainder of the year. The standard deviations from the mean for both sets of data are large, suggesting large variance and a need for more data points for more meaningful results. More data may also produce a clearer pattern for ^{7}Be. In the case of ^{210}Pb, the low in the spring may be a result in increased washout from precipitation, or reduced exhalation of radon from ground saturated with water after the spring thaw.

The activities of both ^{7}Be and ^{210}Pb are not strongly correlated with precipitation on either the full data set or a monthly time scale. There are some indications that large precipitation amounts produce a wash out effect, as there are periods where high precipitation correspond to low radionuclide activity. No correlation between precipitation and radionuclide concentrations is consistent with some of the literature. There is also no clear correlation between the mass of aerosols collected by the air filters and the activity of either radionuclide. The mass collected does vary over time, so that it has no effect on the activities detected in the air filters shows that the changes over time of the activities are independent of the air sampling process itself, and due to other, environmental factors.

The efficiencies measured for the air filters average to around 75% when calculated using the activities of both ^{7}Be and ^{210}Pb. These efficiency values differ greatly from the known efficiency of the air filters (>97% for particles larger than 0.2 μm in size). This discrepancy may originate from incorrect assumptions in the model not taking particle size into account at all, or it may indicate that a portion of roughly 25% of the radionuclides studied absorb onto aerosol particles smaller than 0.2 μm in size. Due to the background count from the lead shielding surrounding the gamma ray detector and small peaks on the lower filters in the stack, the efficiency results for ^{210}Pb have high uncertainties from counting statistics. Therefore, ^{7}Be is a better choice for this method, since it has a higher overall

concentration in the air, resulting in lower counting uncertainties and larger, easily identifiable peaks on both filters.

5.2 Further Research

Further investigation of the nuclide data and relation to additional weather data is warranted. Particularly, an investigation of air mass origin during the sampling time and changes in nuclide activity would be worth undertaking, with the expectation that, as Orono is located in a relatively coastal area, air masses originating over the Atlantic ocean would have less ^{210}Pb than those originating over land. Back trajectory analysis of the air flows occurring during each air sampling period and subsequent classification into groups based on the direction of the air flow would allow the correlation of those groups with parts of the radionucldie data such as the overall activity of either ^{7}Be or ^{210}Pb, or the ratio between the two radionuclide activities, to determine what effect, if any, air mass origin has on the airborne radionuclide measurements. Comparison with other weather variables, such as air temperature, are also possible, although since the air temperature roughly tracks the seasons, there may be little additional information to be gained.

The ^{7}Be data was used as-is, and no considerations were made with regards to the 11-year solar cycle. A second look at the data with the solar cycle taken into account is warranted, to examine any expected correlations, or to remove any effects from the solar cycle's influence from the data, particularly before comparison with the ^{210}Pb data.

Since the US EPA RadNet program represents a large network of air sampling sites across the United States, further collaboration with the EPA or with other air sampling sites on ^{7}Be and ^{210}Pb data would provide further insight into the behavior of both radionuclides. Time series measurements at stations would provide further insight into air mass origin, and the potential to track if certain changes in airborne radionuclide concentrations across a region are due to the same air flow or event.

REFERENCES

Alnour, A., Wagiran, H., Ibrahim, N., Hamzah, S., Siong, W. B., Elias, M. S., 2014. New approach for calibrating the efficiency of HpGe detectors, AIP Conference Proceedings 1584, 38.

Appleby, P. G., Oldfield F., 1978. The Calculation of lead-210 dates assuming a constant rate of supply of unsupported ^{210}Pb to the sediment, CATENA 5, 1-8.

Balkanski, Y. J., Jacob, D. J., Gardner, G. M., Graustein W. C., and Turkenian, K. K., 1993. Transport and Residence Times of Tropospheric Aerosols Inferred from a Global Three-Dimensional Simulation of ^{210}Pb, Journal of Geophysical Research 98, 20573-20586.

Baskaran, M, Coleman, C. H., and Stantschi, P. H., 1993. Atmospheric depositional fluxes of ^{7}Be and ^{210}Pb at Galveston and College Station, Texas, Journal of Geophysical Research 98, 20555-20571.

Baskaran, M., 2011. Po-210 and Pb-210 as atmospheric tracers and global atmospheric Pb-210 fallout: a Review. Journal of Environmental Radioactivity, 500-513.

Bodemann, R., Lange, H.-J., Leya, I., Michel, R., Schiekel, T., Rösel, R., Herpers, U., Hofmann, H.J., Dittrich, B., Suter, M., Wölfli, W., Holmqvist, B., Condé, H., Malmborg, P., 1993. Production of residual nuclei by proton-induced reactions on C, N, O, Mg, Al, and Si. Nuclear Instruments and Methods in Physics Research B 82, 9-31.

Bourcier, L., Masson, O., Laj, P., Pichon, J.M., Paulat, P., Freney, E., Sellegri, K., 2011. Comparative trends and seasonal variation of ^{7}Be, ^{210}Pb and ^{137}Cs at two altitude sites in the central part of France. Journal of Environmental Radioacitivty 102, 294-301.

Climate Change Institute. Images from Climate Reanalyzer (https://ClimateReanalyzer.org), Climate Change Institute, University of Maine, USA. Retrieved May 23, 2022.

David, J.-C., 2015. Spallation reactions: a successful interplay between modeling and applications. European Physical Journal A 51.

Dueñas, C., Orza, J.A.G., Cabello, M., Fernández, M.C., Cañete, S., Pérez, M., Gordo, E., 2011. Air mass origin and its influence on radionuclide activities (^{7}Be and ^{210}Pb) in aerosol particles at a coastal site in the western Mediterranean. Atmospheric Research 101, 205-214.

Hathaway, Amber Emily, "Radiometric Dating: A New Technique" (2020). *Electronic Theses and Dissertations*. 3214. https://digitalcommons.library.umaine.edu/etd/3214

Hersbach, H., Bell, B., Berrisford, P., Biavati, G., Horányi, A., Muñoz Sabater, J., Nicolas, J., Peubey, C., Radu, R., Rozum, I., Schepers, D., Simmons, A., Soci, C., Dee, D., Thépaut, J-N. (2019): ERA5 monthly averaged data on single levels from 1979 to present. Copernicus Climate Change Service (C3S) Climate Data Store (CDS). (Accessed on 23-05-2022), 10.24381/cds.f17050d7

Ioannidou, A., Manolopoulou, M., Papastefanou, C., 2005. Temporal changes of ^{7}Be and ^{210}Pb concentrations in surface air at temperate latitudes (40° N). Applied Radiation and Isotopes 63, 277-284.

Lal, D., Peters, B., 1962. Cosmic ray produced isotopes and their application to problems in geophysics. Progress in Elementary Particle Cosmic Ray Physics 6, 77-243.

Landis, J. D., Renshaw, C. E., and Kaste, J. M., 2021. Sorption Behavior and Aerosol-Particulate Transitions of ^{7}Be, ^{10}Be, and ^{210}Pb: A Basis for Fallout Radionuclide Chronometry. Environmental Science and Technology 55, 14957-14967.

Likuku, A. S., 2006. Factors influencing ambient concentrations of ^{210}Pb and ^{7}Be over the city of Edinburgh (55.9° N, 03.2° W). Journal of Environmental Radioactivity 87, 289-304.

Masarik, J., Beer, J., 1999. Simulation of particle fluxes and cosmogenic nuclide production in the Earth's atmosphere. Journal of Geophysical Research 104, 12,099-12,111.

McFarland, R. C., 1991. Behavior of several germanium detector full-energy-peak efficiency curve-fitting functions. Radioactivity & Radiochemistry The Counting Room: Special Edition, 35-40.

McHargue, L. R., Damon, P. E., 1991. The Global Beryllium 10 Cycle. Reviews of Geophysics 29, 141-158.

Megumi, K., Matsunami, T., Ito, N., Kiyoda, S., Mizohata, A., Asano, T., 2000. Factors, especially sunspot number, causing variations in surface air concentrations and depositions of ^{7}Be in Osaka, Japan. Geophysical Research Letters 27, 361-364.

Menne, Matthew J., Imke Durre, Bryant Korzeniewski, Shelley McNeill, Kristy Thomas, Xungang Yin, Steven Anthony, Ron Ray, Russell S. Vose, Byron E.Gleason, and Tamara G. Houston (2012): Global Historical Climatology Network - Daily (GHCN-Daily), Version 3. Daily Summaries from 2014-01-01 to 2019-06-24, stations GHCND:USW00094644 , GHCND:USW00014606. NOAA National Climatic Data Center. doi:10.7289/V5D21VHZ Accessed 02/09/2022.

Menne, Matthew J., Imke Durre, Russell S. Vose, Byron E. Gleason, and Tamara G. Houston, 2012: An Overview of the Global Historical Climatology Network-Daily Database. J. Atmos. Oceanic Technol., 29, 897-910. doi:10.1175/JTECH-D-11-00103.1.

National Council on Radiation Protection and Measurements. NCRP Report No. 160 Ionizing Radiation Exposure of the Population of the Unites States. 2009.

O'Brien, K., 1979. Secular Variations in the production of cosmogenic isotopes in the Earth's atmosphere. Journal of Geophysical Research 84, 423-431.

Papastefanou, C. and Ioannidou, A., 1995. Aerodynamic Size Association of ^{7}Be in Ambient Aerosols. Journal of Enbironmental Radioactivity 26, 273-282.

Persson, B. R. R., 2015, Global distribution of ^{7}Be, ^{210}Pb, and ^{210}Po in the surface air. Acta Scientiarum Ludensia, Vol. 2015-008, 1-24.

Persson B. R. R., 1970. ^{55}Fe, ^{90}Sr, ^{134}Cs, and ^{210}Pb in the Biosphere. Radiological Health Aspects of the Environmental Contamination from Radioactive Materials in Northern Sweden, PhD thesis, Lund University, Lund, Sweden.

Renfro, A. A., Cochran, J. K., Colle, B. A., 2013. Atmospheric fluxes of ^{7}Be and ^{210}Pb on monthly time-scales and during rainfall events at Stony Brook, New York (USA). Journal of Environmental Radioactivity 116, 114-123.

Sisterson, J.M., Kim, K., Beverding, A., Englert, P.A.J., Caffee, M., Jull, A.J.T., Donahue, D.J., McHargue, L., Castaneda, C., Vincent, J., Reedy, R.C., 1997. Measurement of proton production cross sections of ^{10}Be and ^{26}Al from elements found in lunar rocks. Nuclear Instruments and Methods in Physics Research B 123, 324-329.

Terzi, L., Kalinowski, M., 2017. World-wide seasonal variation of ^{7}Be related to large-scale atmospheric circulation dynamics. Journal of Environmental Radioactivity 178-179, 1-15.

Todorovic, D., Popovic, D., Djuric, G., Radenkovic, M., 2005. ^{7}Be to ^{210}Pb concentration ratio in ground level air in Belgrade area. Journal of Environmental Radioactivity 79, 297-307.

Tokieda, T., Yamanaka, K., Harada, K, and Tsunogai, S, 1996. Seasonal variations of residence time and upper atmospheric contribution of aerosols studied with Pb-210, Bi-210, Po-210, and Be-7. Tellus 48B, 690-702.

Usoskin, I. G., Kovaltsov G. A., 2008. Production of cosmogenic ^{7}Be isotope in the atmosphere: Full 3-D modeling. Journal of Geophysical Research 113, D12107.

Webber, W. R., Higbie, P. R., McCracken, K. G., 2007. Production of the cosmogenic isotopes ^{3}H, ^{7}Be, ^{10}Be, and ^{36}Cl in the Earth's atmosphere by solar and galactic cosmic rays. Journal of Geophysical Research 112, A10106

Yoshimori, M., 2005. Production and behavior of beryllium 7 radionuclide in the upper atmosphere. Advances in Space Research 36, 922-926.

APPENDIX A: FULL DATA TABLES

In the following pages, the full tabulated data are collected.

Table A.1 contains the full data used in plotting the activity of ^{210}Pb and ^{7}Be over time. The time elapsed column shows the time, in days, between the end date of the air sampling run, and the date the filter was counted. The ^{7}Be activity at end date column shows the back-calculated activity of ^{7}Be at the end of the air sampling run, based on the elapsed time between the end of the run and the date the filter was counted.

Table A.2 contains the full set of data averaged over each month.

Table A.3 contains the full set of data for mass collected on air sample filters.

Table A.4 contains the full set of weather data collected from the NOAA Climate Data Online archive of GCHN-Daily data for Bangor International Airport (Menne, 2012 and Menne 2022).

Table A.1: Full activity data for ^{210}Pb and ^{7}Be from February 2014 to June 2019.

Sample End Date	Date Filter Counted	Time elapsed (days)	^{210}Pb Activity (Bq)	^{210}Pb Uncertainty (%)	^{7}Be Activity (Bq)	^{7}Be Activity at end date (Bq)	^{7}Be Uncertainty (%)
2/13/2014	7/24/2014	161	3.631	6.1	2.167	17.587	7.3
2/27/2014	7/15/2014	138	4.181	5.7	3.965	23.859	5.0
3/16/2014	7/14/2014	120	2.213	8.2	3.844	18.304	5.0
3/28/2014	7/11/2014	105	4.469	5.5	6.936	27.173	3.6
4/9/2014	7/10/2014	92	2.230	8.3	6.563	21.714	3.7
4/16/2014	7/9/2014	84	3.777	6.1	10.339	30.824	2.9
4/23/2014	7/8/2014	76	2.737	7.3	7.975	21.427	3.4
5/2/2014	7/3/2014	62	0.924	12.3	2.950	6.608	6.0
5/12/2014	7/2/2014	51	1.869	8.7	6.708	13.021	3.6
5/28/2014	7/17/2014	50	0.473	16.0	4.462	8.549	4.5
6/6/2014	7/21/2014	45	2.110	8.8	17.458	31.343	2.1
6/15/2014	9/5/2014	82	0.997	11.6	3.537	10.275	5.3
6/23/2014	9/8/2014	77	1.259	10.9	4.921	13.395	4.3
6/30/2014	9/7/2014	69	1.908	8.9	14.818	36.348	2.3
7/7/2014	9/4/2014	59	2.411	7.7	12.050	25.955	2.6
7/16/2014	9/3/2014	49	2.295	8.1	12.175	23.025	2.6
8/20/2014	3/4/2015	196	1.448	9.7	0.718	9.183	16.7
9/11/2014	3/30/2015	200	2.406	7.5	1.694	22.834	8.6
9/18/2014	3/26/2015	189	1.590	9.6	1.598	18.661	8.8
9/26/2014	3/24/2015	179	2.003	8.3	1.460	14.970	9.8
10/1/2014	3/20/2015	170	1.560	9.5	1.235	11.270	11.2
10/19/2014	3/18/2015	150	1.478	10.1	1.515	10.655	9.3
11/1/2014	3/17/2015	136	1.869	8.8	2.623	15.376	6.6
11/12/2014	3/16/2015	124	1.908	8.8	2.916	14.626	6.0
11/24/2014	3/12/2015	108	1.440	10.1	3.006	12.244	6.0
12/31/2014	1/29/2015	29	2.342	7.7	7.443	10.853	3.5
1/11/2015	2/2/2015	22	3.029	6.4	10.273	13.676	3.1
02/04/15	07/28/15	174	9.942	3.5	6.067	58.300	3.9
02/18/15	07/27/15	159	8.099	3.9	3.644	28.813	5.3
02/27/15	07/24/15	147	6.862	4.3	3.133	21.195	5.8

Table A.1 Continued.							
03/20/15	07/23/15	125	2.866	7.2	4.690	23.830	4.5
04/26/15	08/03/15	99	1.096	11.5	3.758	13.617	5.2
05/28/15	07/30/15	63	4.086	5.8	17.882	40.573	2.1
06/17/15	07/29/15	42	1.594	9.7	11.274	19.466	2.7
07/09/15	08/04/15	26	1.195	11.4	12.026	16.864	2.7
08/28/15	08/31/15	3	1.869	8.9	14.921	15.515	2.4
09/09/15	09/09/15	0	2.969	7.4	13.586	13.586	2.5
09/17/15	09/18/15	1	2.479	7.9	16.498	16.714	2.2
09/27/15	09/28/15	1	2.196	8.5	14.324	14.512	2.4
10/06/15	10/06/15	0	1.616	11.5	16.353	16.353	2.3
10/15/15	10/16/15	1	7.394	4.8	51.569	52.244	1.2
10/24/15	10/26/15	2	3.120	4.9	23.348	23.964	1.3
11/03/15	11/04/15	1	1.899	6.3	11.541	11.692	1.9
11/12/15	11/13/15	1	8.532	4.0	31.377	31.788	1.8
11/20/15	11/23/15	3	2.725	7.2	20.402	21.214	2.3
11/29/15	12/01/15	2	2.855	10.4	30.715	31.525	1.8
12/03/15	12/04/15	1	1.817	9.3	7.374	7.471	4.2
12/12/15	12/14/15	2	6.602	4.5	25.491	26.163	2.0
12/24/15	01/22/16	29	1.882	12.0	10.406	15.173	4.8
01/02/16	01/25/16	23	3.861	8.5	24.555	33.117	2.9
01/13/16	01/26/16	13	4.692	7.7	30.450	36.058	2.6
01/24/16	01/28/16	4	5.197	7.3	53.386	56.237	1.9
02/04/16	02/04/16	0	2.232	6.8	24.278	24.278	1.9
02/12/16	02/18/16	6	11.639	5.4	91.425	98.844	1.5
02/24/16	02/26/16	2	1.552	7.6	22.439	23.030	2.1
03/06/16	03/08/16	2	3.298	6.3	37.528	38.517	1.6
03/17/16	03/17/16	0	3.557	3.7	50.508	50.508	1.2
03/25/16	03/29/16	4	2.900	4.0	58.323	61.437	1.1
04/05/16	04/06/16	1	3.236	3.8	51.166	51.836	1.2
04/14/16	04/15/16	1	1.744	4.8	46.404	47.011	1.3
04/27/16	04/27/16	0	4.749	3.5	98.289	98.289	0.9
05/05/16	05/06/16	1	1.516	5.0	59.769	60.552	1.2

Table A.1 Continued.							
05/15/16	05/16/16	1	2.012	4.7	52.467	53.154	1.3
05/24/16	05/26/16	2	3.014	4.1	61.608	63.231	1.2
06/03/16	06/06/16	3	1.332	5.1	27.313	28.399	1.8
06/14/16	06/15/16	1	1.467	5.0	25.778	26.115	1.8
06/23/16	06/28/16	5	0.832	5.6	13.593	14.506	2.5
07/02/16	07/05/16	3	2.403	4.4	43.141	44.857	1.4
07/13/16	07/14/16	1	1.149	5.3	23.990	24.304	1.9
07/22/16	07/25/16	3	2.021	4.7	22.995	23.910	1.9
08/03/16	08/03/16	0	0.196	6.5	18.880	18.880	2.1
08/12/16	08/12/16	0	0.164	6.5	27.127	27.127	1.8
08/20/16	08/23/16	3	2.265	4.5	38.815	40.359	1.5
08/31/16	09/07/16	7	1.878	3.9	22.020	24.118	1.3
09/15/16	09/16/16	1	0.941	4.8	12.440	12.603	1.7
09/24/16	09/26/16	2	2.299	3.7	16.088	16.512	1.5
10/04/16	10/06/16	2	0.774	5.0	12.230	12.552	1.7
10/15/16	10/21/16	6	1.740	4.0	16.916	18.289	1.4
10/28/16	10/31/16	3	0.834	5.0	5.822	6.053	2.4
11/09/16	11/09/16	0	2.196	3.7	22.151	22.151	1.2
11/17/16	11/18/16	1	1.251	4.4	15.701	15.907	1.5
11/27/16	11/28/16	1	0.353	5.8	2.702	2.737	3.6
12/01/16	12/05/16	4	0.091	6.5	1.118	1.178	5.6
12/09/16	12/09/16	0	2.995	3.3	31.606	31.606	1.0
12/17/16	12/27/16	10	4.219	2.9	16.236	18.491	1.5
01/18/17	01/18/17	0	6.097	2.5	48.177	48.177	0.8
01/27/17	01/27/17	0	1.964	3.9	18.824	18.824	1.4
02/04/17	02/06/17	2	4.103	2.9	25.374	26.043	1.2
02/14/17	02/15/17	1	4.542	2.8	25.992	26.332	1.2
02/24/17	02/27/17	3	5.478	2.6	65.614	68.224	0.7
03/08/17	03/08/17	0	5.268	2.6	49.416	49.416	0.8
03/17/17	03/17/17	0	5.104	2.7	27.758	27.758	1.1
03/25/17	03/26/17	1	6.780	2.4	63.464	64.295	0.7
04/03/17	04/03/17	0	3.059	3.3	40.081	40.081	0.9

Table A.1 Continued.							
04/11/17	04/12/17	1	2.505	3.5	33.846	34.289	1.0
04/20/17	04/26/17	6	3.296	3.2	40.571	43.864	0.9
05/02/17	05/02/17	0	1.186	4.5	25.930	25.930	1.2
05/11/17	05/11/17	0	1.676	4.1	16.802	16.802	1.4
05/20/17	05/20/17	0	1.255	4.4	30.661	30.661	1.1
05/28/17	05/30/17	2	0.731	5.1	13.158	13.505	1.6
06/07/17	06/19/17	12	0.662	5.2	19.031	22.246	1.3
06/19/17	06/20/17	1	3.463	3.1	48.608	49.245	0.8
06/27/17	06/28/17	1	2.767	3.4	57.698	58.453	0.8
07/06/17	07/10/17	4	3.515	3.1	48.822	51.429	0.8
07/16/17	07/17/17	1	3.592	3.1	67.436	68.319	0.7
07/25/17	07/26/17	1	3.317	3.2	42.414	42.969	0.9
08/03/17	08/04/17	1	3.094	3.3	44.043	44.619	0.9
08/13/17	08/14/17	1	3.029	3.3	47.314	47.934	0.9
08/23/17	08/23/17	0	2.664	3.5	40.537	40.537	0.9
08/31/17	09/01/17	1	2.690	3.5	44.975	45.563	0.9
09/11/17	09/11/17	0	3.412	3.1	37.069	37.069	1.0
09/18/17	09/18/17	0	4.945	2.7	40.551	40.551	0.9
09/26/17	09/26/17	0	4.984	2.7	41.865	41.865	0.9
10/05/17	10/05/17	0	3.167	3.2	51.100	51.100	0.8
10/14/17	10/16/17	2	3.665	3.1	35.564	36.501	1.0
10/24/17	10/24/17	0	2.303	3.7	54.444	54.444	0.8
11/08/17	11/14/17	6	4.176	2.9	33.014	35.693	1.0
11/18/17	11/20/17	2	3.455	3.1	25.177	25.841	1.2
11/29/17	11/29/17	0	4.447	2.8	35.392	35.392	1.0
12/07/17	12/18/17	11	2.458	3.6	29.615	34.169	1.1
12/17/17	12/29/17	12	2.325	3.6	23.721	27.727	1.2
12/27/17	01/02/18	6	3.047	3.3	28.859	31.201	1.1
01/07/18	01/07/18	0	6.140	2.5	33.642	33.642	1.0
01/16/18	01/16/18	0	8.486	2.1	38.894	38.894	0.9
02/03/18	02/28/18	25	3.794	3.0	23.704	32.810	1.2
02/22/18	03/01/18	7	2.948	3.3	32.058	35.113	1.0

Table A.1 Continued.							
03/09/18	03/16/18	7	0.662	5.2	21.968	24.062	1.3
03/18/18	03/30/18	12	2.041	3.8	18.341	21.439	1.4
03/28/18	04/13/18	16	1.470	4.2	22.876	28.167	1.2
04/15/18	04/24/18	9	4.052	2.9	32.945	37.036	1.0
05/09/18	05/14/18	5	3.296	3.2	49.537	52.865	0.8
06/01/18	06/01/18	0	3.283	3.2	62.008	62.008	0.7
06/10/18	06/12/18	2	2.295	3.7	38.049	39.051	1.0
06/20/18	07/02/18	12	3.437	3.1	43.108	50.388	0.9
06/29/18	07/03/18	4	2.509	3.5	67.971	71.600	0.7
07/18/18	07/25/18	7	3.717	3.0	46.000	50.383	0.9
08/01/18	08/01/18	0	4.202	2.9	43.608	43.608	0.9
08/10/18	08/10/18	0	13.637	1.7	89.176	89.176	0.6
08/18/18	08/23/18	5	4.692	2.8	39.067	41.691	0.9
08/31/18	09/04/18	4	5.495	2.6	44.850	47.245	0.9
09/12/18	09/18/18	6	3.175	3.2	35.864	38.775	1.0
09/26/18	09/26/18	0	1.869	3.9	23.428	23.428	1.2
10/07/18	10/10/18	3	3.214	3.2	38.135	39.652	1.0
10/18/18	10/19/18	1	2.226	3.7	29.815	30.205	1.1
10/27/18	10/30/18	3	2.737	3.4	34.425	35.795	1.0
11/09/18	11/09/18	0	1.560	4.2	13.438	13.438	1.6
11/18/18	11/19/18	1	2.149	3.7	18.472	18.714	1.4
11/27/18	11/29/18	2	6.853	2.4	32.452	33.307	1.0
12/07/18	12/10/18	3	2.729	3.4	20.560	21.378	1.3
12/19/18	12/27/18	8	5.057	2.7	23.404	25.970	1.2
01/05/19	01/07/19	2	2.647	3.5	27.586	28.313	1.1
01/16/19	01/25/19	9	1.895	3.9	22.013	24.746	1.3
02/04/19	02/04/19	0	1.624	4.1	27.872	27.872	1.1
02/13/19	02/18/19	5	3.854	3.0	40.292	42.999	0.9
02/25/19	02/25/19	0	3.983	3.0	56.062	56.062	0.8
03/06/19	03/07/19	1	4.447	2.8	67.322	68.203	0.7
03/16/19	03/27/19	11	4.825	2.7	42.883	49.478	0.9
04/04/19	04/16/19	12	2.806	3.4	43.518	50.868	0.9

Table A.1 Continued.							
04/27/19	05/14/19	17	1.160	4.5	9.662	12.053	1.9
05/22/19	06/10/19	19	1.178	4.5	10.349	13.250	1.8
06/07/19	06/07/19	0	2.024	3.8	38.332	38.332	0.9
06/16/19	06/16/19	0	0.654	5.2	28.756	28.756	1.1
06/24/19	06/25/19	1	1.839	3.9	28.245	28.615	1.1

Table A.2: Averaged ^{210}Pb and ^{7}Be data for each month of the study. Each month is indicated in MM/YYYY format. The data is split into columns for better use of space.

Month	^{210}Pb (Bq)	^{7}Be (Bq)	Month	^{210}Pb (Bq)	^{7}Be (Bq)
02/2014	3.91	20.7	01/2017	2.69	22.3
03/2014	3.34	22.7	02/2017	4.71	40.2
04/2014	2.91	24.7	03/2017	5.72	47.2
05/2014	1.09	9.39	04/2017	2.95	39.4
06/2014	1.57	22.8	05/2017	1.21	21.7
07/2014	2.35	24.5	06/2017	2.30	43.3
08/2014	1.45	9.18	07/2017	3.47	54.2
09/2014	1.20	18.8	08/2017	2.87	44.7
10/2014	1.52	11.0	09/2017	4.45	39.8
11/2014	1.74	14.1	10/2017	3.05	47.3
12/2014	2.34	10.9	11/2017	4.03	32.3
01/2015	3.03	13.7	12/2017	2.61	31.0
02/2015	8.30	36.1	01/2018	7.31	36.3
03/2015	2.87	23.8	02/2018	5.27	50.4
04/2015	1.10	13.6	03/2018	1.39	24.6
05/2015	4.09	40.6	04/2018	4.05	37.0
06/2015	1.59	19.5	05/2018	3.29	57.4
07/2015	1.19	16.7	06/2018	2.75	53.7
08/2015	1.87	15.5	07/2018	3.96	47.0
09/2015	2.55	14.9	08/2018	7.94	59.4
10/2015	4.04	30.9	09/2018	2.52	31.1
11/2015	4.00	24.1	10/2018	2.73	35.2

Table A.2 Continued.

12/2015	3.43	16.3	11/2018	3.52	21.8
01/2016	4.58	41.8	12/2018	3.89	23.7
02/2016	5.14	48.7	01/2019	2.27	26.5
03/2016	3.25	50.2	02/2019	3.15	42.3
04/2016	3.24	65.7	03/2019	4.64	58.8
05/2016	2.18	59.0	04/2019	1.98	31.5
06/2016	1.21	23.0	05/2019	1.18	13.2
07/2016	1.86	31.0	06/2019	1.51	31.9
08/2016	1.13	27.6			
09/2016	1.62	14.6			
10/2016	1.12	12.3			
11/2016	1.27	13.6			
12/2016	2.44	17.1			

Table A.3: Air filter mass data.

Date filter was collected	Initial filter mass (g)	Final filter mass (g)	Collected mass (g)
09/28/15	4.206	4.3289	0.1229
10/06/15	4.3656	4.4424	0.0768
10/15/15	3.9008	3.9981	0.0973
10/24/15	3.949	4.0545	0.1055
11/04/15	3.9447	4.0272	0.0825
11/12/15	3.7512	3.9521	0.2009
11/20/15	4.3186	4.3964	0.0778
11/30/15	4.1128	4.2001	0.0873
12/03/15	3.5538	3.5772	0.0234
02/12/16	3.9685	4.0495	0.081
02/24/16	4.0945	4.2491	0.1546
03/06/16	4.2723	4.4668	0.1945
03/16/16	4.2017	4.346	0.1443
03/28/16	3.8045	3.9094	0.1049
04/05/16	4.0426	4.1986	0.156

Table A.3 Continued.			
04/15/16	3.9259	4.0575	0.1316
04/27/16	3.9095	4.1569	0.2474
05/06/16	3.7758	3.9033	0.1275
05/16/16	4.6913	4.8567	0.1654
05/26/16	4.4784	4.6797	0.2013
06/06/16	4.064	4.339	0.275
06/15/16	4.4481	4.7666	0.3185
06/24/16	4.046	4.2644	0.2184
07/05/16	3.9127	3.9893	0.0766
07/14/16	3.6323	3.6993	0.067
07/25/16	3.9736	4.0519	0.0783
08/03/16	3.9354	4.0022	0.0668
08/12/16	3.8876	3.9841	0.0965
08/23/16	3.9048	3.9551	0.0503
09/06/16	4.4538	4.5751	0.1213
09/15/16	4.2629	4.3381	0.0752
09/26/16	4.2085	4.2913	0.0828
10/06/16	4.3727	4.4368	0.0641
10/19/16	3.9735	4.051	0.0775
10/31/16	4.3357	4.3806	0.0449
11/09/16	4.0987	4.1797	0.081
11/18/16	3.9965	4.0687	0.0722
11/28/16	3.9669	3.9895	0.0226
01/27/17	4.2028	4.2694	0.0666
02/06/17	4.1996	4.4689	0.2693
02/15/17	4.0986	4.2069	0.1083
02/27/17	4.113	4.2459	0.1329
02/27/17	4.2368	4.2528	0.016
03/08/17	4.4563	4.6851	0.2288
03/17/17	4.383	4.5861	0.2031
03/26/17	4.1906	4.3732	0.1826
03/26/17	4.2115	4.2293	0.0178

Table A.3 Continued.			
04/03/17	4.2409	4.3571	0.1162
04/12/17	4.0082	4.2977	0.2895
04/24/17	4.1728	4.4488	0.2760
05/02/17	4.4647	4.642	0.1773
05/11/17	4.1088	4.2203	0.1115
05/20/17	4.2222	4.4467	0.2245
05/30/17	4.0262	4.1864	0.1602
06/08/17	3.8037	4.004	0.2003
06/19/17	4.0039	4.5671	0.5632
06/28/17	3.632	3.805	0.173
07/07/17	4.3561	4.4857	0.1296
07/17/17	4.0901	4.2079	0.1178
07/26/17	4.2408	4.3549	0.1141
08/04/17	3.9432	4.1009	0.1577
08/14/17	4.0049	4.136	0.1311
08/23/17	3.9393	4.0707	0.1314
08/31/17	3.8532	4.0012	0.148
09/11/17	3.7768	3.9709	0.1941
09/18/17	3.8114	3.9573	0.1459
09/26/17	3.9501	4.0981	0.148
10/05/17	3.635	3.8125	0.1775
10/16/17	3.8973	3.9987	0.1014
10/24/17	4.2202	4.3713	0.1511
11/10/17	3.8955	4.0327	0.1372
11/20/17	4.3032	4.3917	0.0885
11/29/17	4.3512	4.4453	0.0941

Table A.4: GCHN-Daily Precipitation data for Bangor International Airport, used in comparison with radionuclide activity data.

End Date	Time elapsed	Precip (mm)	Snow (mm)	Total (mm)
2/13/2014	0	6.9	137	20.6
2/27/2014	14	7.4	3	7.7
3/16/2014	31	37.1	328	69.9
3/28/2014	43	3.6	10	4.6
4/9/2014	55	17.2	3	17.5
4/16/2014	62	26.7	25	29.2
4/23/2014	69	6.4	0	6.4
5/2/2014	78	22.9	0	22.9
5/12/2014	88	3.8	0	3.8
5/28/2014	104	11.3	0	11.3
6/6/2014	113	14.4	0	14.4
6/15/2014	122	19.3	0	19.3
6/23/2014	130	23.7	0	23.7
6/30/2014	137	33	0	33
7/7/2014	144	92.7	0	92.7
7/16/2014	153	48.5	0	48.5
8/20/2014	188	27.1	0	27.1
9/11/2014	210	14.3	0	14.3
9/18/2014	217	6.9	0	6.9
9/26/2014	225	1.3	0	1.3
10/1/2014	230	0.3	0	0.3
10/19/2014	248	47.8	0	47.8
11/1/2014	261	12.2	0	12.2
11/12/2014	272	12.8	0	12.8
11/24/2014	284	22.1	0	22.1
12/31/2014	321	28.7	0	28.7
1/11/2015	332	5.6	102	15.8
02/04/15	356	43.7	703	114
02/18/15	370	4.1	99	14

Table A.4, Continued.				
02/27/15	379	15.2	331	48.3
03/20/15	400	18.8	267	45.5
04/26/15	437	30.8	0	30.8
05/28/15	469	34	0	34
06/17/15	489	24	0	24
07/09/15	511	4.3	0	4.3
08/28/15	561	22.9	0	22.9
09/09/15	573	0.3	0	0.3
09/17/15	581	33.1	0	33.1
09/27/15	591	2.5	0	2.5
10/06/15	600	139.2	0	139.2
10/15/15	609	18.2	0	18.2
10/24/15	618	5.6	0	5.6
11/03/15	628	40.1	0	40.1
11/12/15	637	6.6	0	6.6
11/20/15	645	24.9	0	24.9
11/29/15	654	24.2	64	30.6
12/03/15	658	20.4	0	20.4
12/12/15	667	0.5	0	0.5
12/24/15	679	32.6	0	32.6
01/02/16	688	21.9	231	45
01/13/16	699	54.1	61	60.2
01/24/16	710	1	13	2.3
02/04/16	721	12.5	8	13.3
02/12/16	729	19.6	360	55.6
02/24/16	741	17.6	71	24.7
03/06/16	752	20.6	10	21.6
03/17/16	763	17.8	0	17.8
03/25/16	771	11.7	142	25.9
04/05/16	782	19	0	19
04/14/16	791	52.6	0	52.6
04/27/16	804	0.8	0	0.8

Table A.4, Continued.				
05/05/16	812	21.6	0	21.6
05/15/16	822	21.8	0	21.8
05/24/16	831	0.5	0	0.5
06/03/16	841	5.1	0	5.1
06/14/16	852	37.4	0	37.4
06/23/16	861	3.3	0	3.3
07/02/16	870	34.7	0	34.7
07/13/16	881	22.4	0	22.4
07/22/16	890	19.8	0	19.8
08/03/16	902	0	0	0
08/12/16	911	18	0	18
08/20/16	919	18.6	0	18.6
08/31/16	930	0.5	0	0.5
09/15/16	945	9.7	0	9.7
09/24/16	954	18.1	0	18.1
10/04/16	964	4.9	0	4.9
10/15/16	975	17.7	0	17.7
10/28/16	988	60.2	0	60.2
11/09/16	1000	13	0	13
11/17/16	1008	37.3	0	37.3
11/27/16	1018	28.7	38	32.5
12/01/16	1022	53.8	38	57.6
12/09/16	1030	3.7	46	8.3
12/17/16	1038	13.8	206	34.4
01/18/17	1070	15.3	13	16.6
01/27/17	1079	43.7	30	46.7
02/04/17	1087	1.3	43	5.6
02/14/17	1097	42.2	874	129.6
02/24/17	1107	1.6	0	1.6
03/08/17	1119	15.6	0	15.6
03/17/17	1128	20.4	371	57.5
03/25/17	1136	2.8	43	7.1

Table A.4, Continued.				
04/03/17	1145	13.7	18	15.5
04/11/17	1153	41.7	48	46.5
04/20/17	1162	9.9	10	10.9
05/02/17	1174	61.6	0	61.6
05/11/17	1183	38.1	0	38.1
05/20/17	1192	55.9	0	55.9
05/28/17	1200	31.7	0	31.7
06/07/17	1210	31.5	0	31.5
06/19/17	1222	18.3	0	18.3
06/27/17	1230	35	0	35
07/06/17	1239	26.5	0	26.5
07/16/17	1249	17.8	0	17.8
07/25/17	1258	11.2	0	11.2
08/03/17	1267	3.8	0	3.8
08/13/17	1277	7.8	0	7.8
08/23/17	1287	18.6	0	18.6
08/31/17	1295	0	0	0
09/11/17	1306	51.5	0	51.5
09/18/17	1313	0.5	0	0.5
09/26/17	1321	1.3	0	1.3
10/05/17	1330	0	0	0
10/14/17	1339	23.7	0	23.7
10/24/17	1349	1.3	0	1.3
11/08/17	1364	20.6	0	20.6
11/18/17	1374	15.3	0	15.3
11/29/17	1385	23.9	0	23.9
12/07/17	1393	33.6	0	33.6
12/17/17	1403	21.1	81	29.2
12/27/17	1413	26.7	382	64.9
01/07/18	1424	18.8	468	65.6
01/16/18	1433	71.1	0	71.1
02/03/18	1451	11	107	21.7

Table A.4, Continued.				
02/22/18	1470	10.4	51	15.5
03/09/18	1485	12.3	269	39.2
03/18/18	1494	29.4	546	84
03/28/18	1504	1.5	13	2.8
04/15/18	1522	12.9	0	12.9
05/09/18	1546	25.9	0	25.9
06/01/18	1569	12	0	12
06/10/18	1578	23.1	0	23.1
06/20/18	1588	41.7	0	41.7
06/29/18	1597	60.9	0	60.9
07/18/18	1616	3.9	0	3.9
08/01/18	1630	20.8	0	20.8
08/10/18	1639	26.9	0	26.9
08/18/18	1647	24.5	0	24.5
08/31/18	1660	2	0	2
09/12/18	1672	23.1	0	23.1
09/26/18	1686	41.1	0	41.1
10/07/18	1697	27.7	0	27.7
10/18/18	1708	39.6	0	39.6
10/27/18	1717	35.6	0	35.6
11/09/18	1730	87.9	15	89.4
11/18/18	1739	35.4	115	46.9
11/27/18	1748	28.7	246	53.3
12/07/18	1758	23.6	36	27.2
12/19/18	1770	15.1	170	32.1
01/05/19	1787	18.5	130	31.5
01/16/19	1798	13.2	18	15
02/04/19	1817	9.7	120	21.7
02/13/19	1826	21.1	223	43.4
02/25/19	1838	16.8	152	32
03/06/19	1847	11.2	122	23.4
03/16/19	1857	5.9	48	10.7

Table A.4, Continued.				
04/04/19	1876	24.6	56	30.2
04/27/19	1899	84.8	0	84.8
05/22/19	1924	41.7	0	41.7
06/07/19	1940	8.5	0	8.5
06/16/19	1949	31	0	31
06/24/19	1957	44.4	0	44.4

APPENDIX B: LARGE GRAPHS

Appendix B contains large time-series plots of some of the data, printed in landscape format. Figure B.1 shows the activity of both ^{7}Be and ^{210}Pb for the entire sampling period. Figures B.2 and B.3 show the total precipitation during each sampling period and the corresponding activity of ^{7}Be and ^{210}Pb, respectively. The data begins at t=0 days on February 13, 2014, and ends on June 24, 2019, in all three plots.

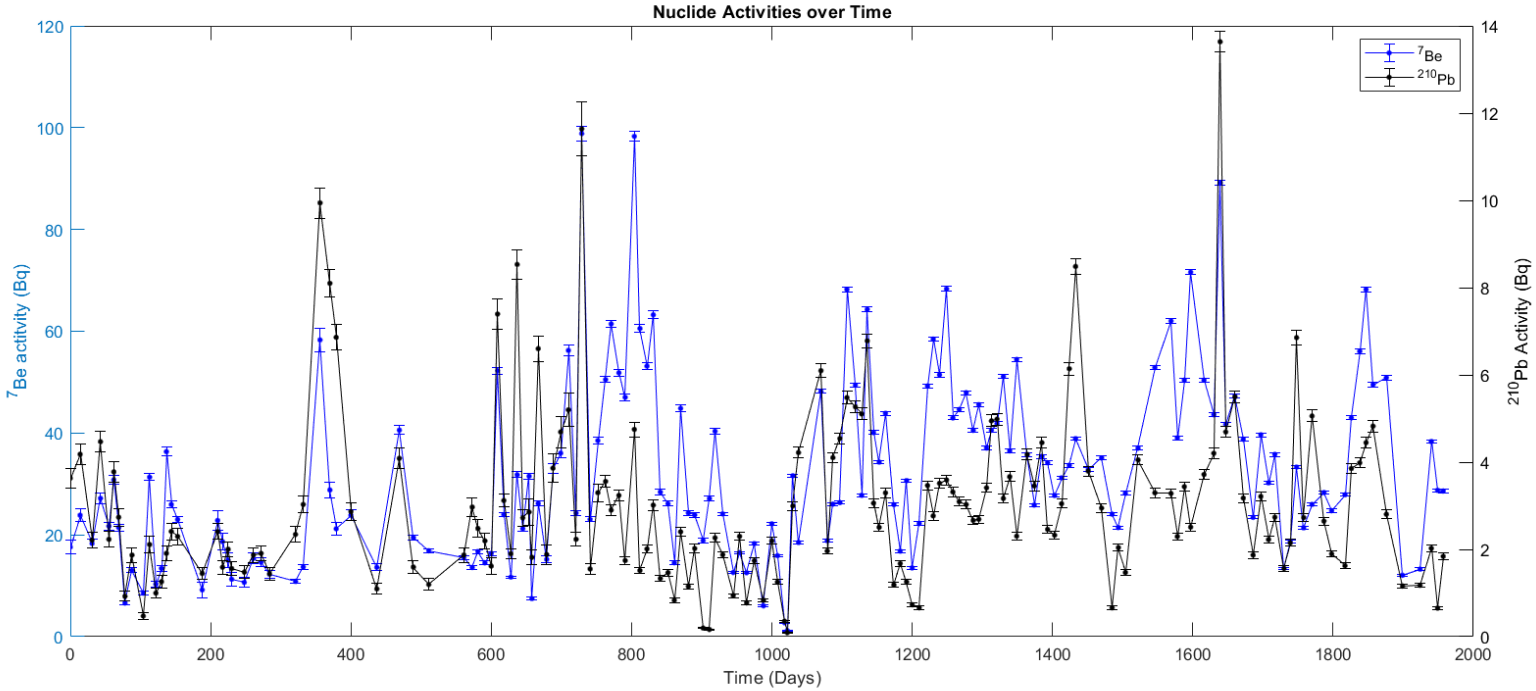

Figure B.1: ^{7}Be and ^{210}Pb activities over time. This is the same plot as in Fig. 3.1, enlarged for easier reading. The error bars on the data points represent the uncertainty from counting statistics.

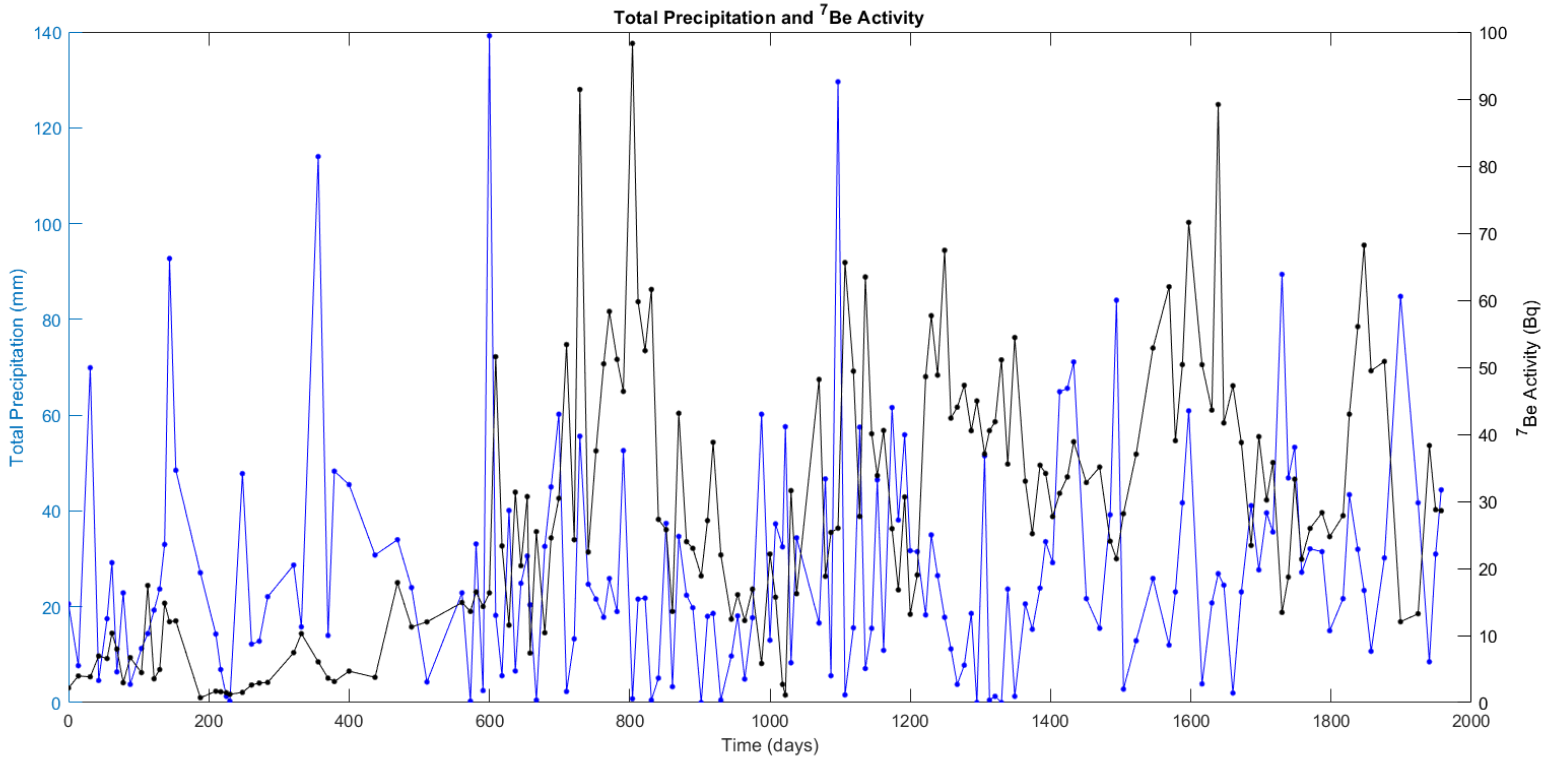

Figure B.2: Total precipitation and ^{7}Be activity. This figure displays the same data as Fig. 3.11, on a single continuous axis.

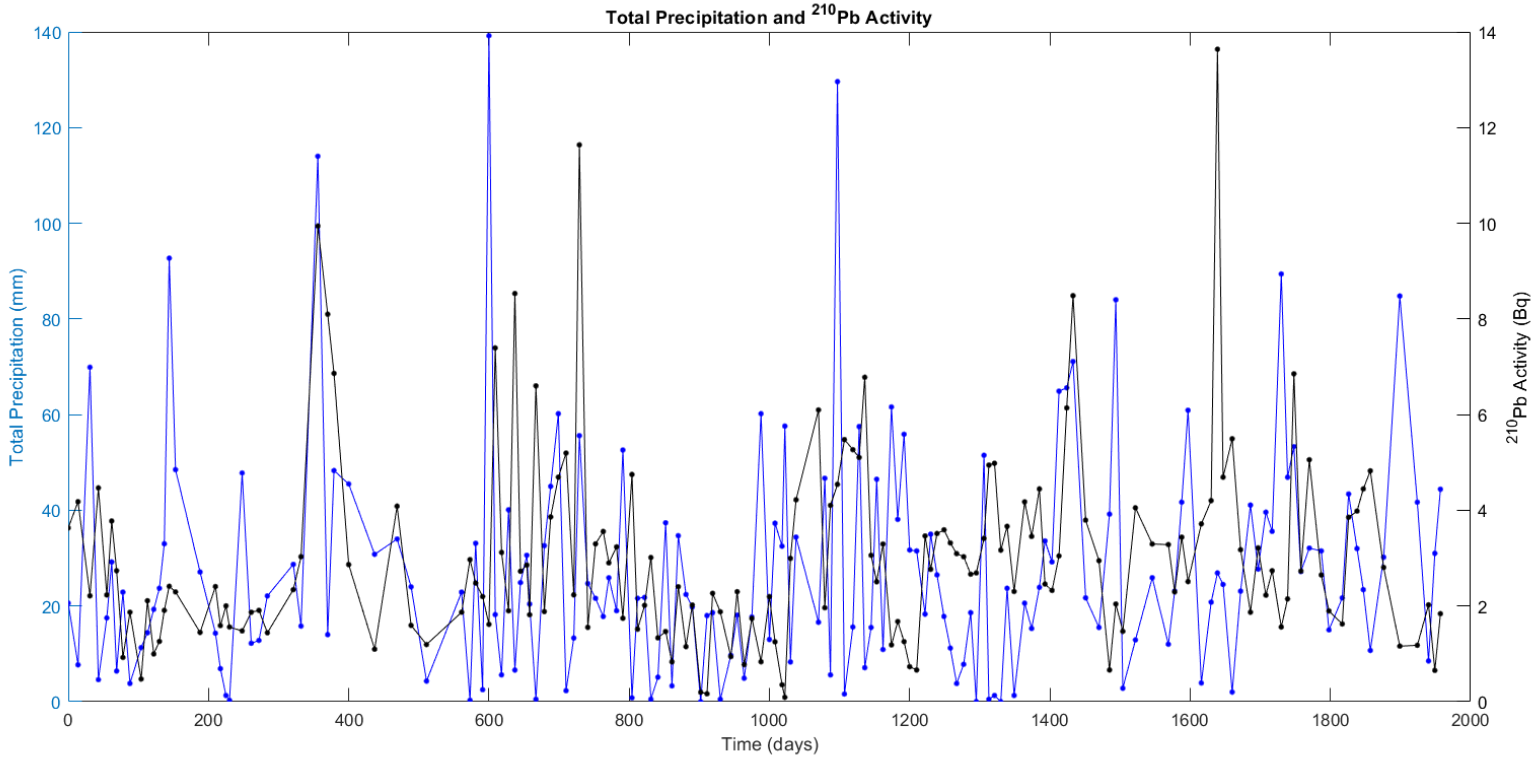

Figure B.3: Total precipitation and ^{210}Pb activity. This figure shows the same data as Fig. 3.10, on a single continuous axis.

APPENDIX C: EXPLANATION OF DIGITAL ARCHIVE

Included with this thesis is a compact disk containing a copy of all data files involved in the research. The MAESTRO spectrum files folder contains spectrum files for all data collected using MAESTRO, saved in .spe format. The filenames for data runs are the end date of the air sampling run for the filter, in YYYYMMDD format, followed by any comments in text (for example, “20160603 top filter.spe” for the top filter in the stack of filters collected on 06/03/2016). Background spectra are saved with a prefix of “bkg” followed by the date the background was taken in YYYYMMDD format (example: “bkg20160612.spe”). The other files are calibration spectra saved with a descriptive filename.

BIOGRAPHY OF AUTHOR

James William Deaton was born in Saint Augustine, Florida, on July 2, 1985. From the age of two onward, he grew up in Lafayette, Louisiana. He graduated from Lafayette High School in 2003. After high school, he attended The University of Florida (UF), majoring in mechanical engineering, until he transferred to the University of Louisiana at Lafayette (ULL) in 2006, and changed his major to physics. He graduated from ULL in 2008, with a Bachelor of Science degree in Physics. He remained at ULL to pursue a Master of Science (non-thesis) degree in Physics, graduating in 2010.

James entered the Physics and Astronomy graduate program at the University of Maine in 2013. At the University of Maine, he was honored to receive the College of Engineering Graduate Assistant Teaching Award in 2019, and the College of Liberal Arts and Sciences Outstanding Graduate Student in 2021, both for his work as a teaching assistant. He has been the instructor of record for PHY 111 or PHY 112 for the summers of 2016, 2017, and 2018, and the instructor of record for PHY 470 and 471 in 2021 and 2022. James is a candidate for the Doctor of Philosophy degree in Physics from The University of Maine in August 2022.